Contribution of early Alzheimer's disease-related pathophysiology to the development of acquired epilepsy

Gschwind, Tilo ; Lafourcade, Carlos ; Gfeller, Tim ; Zaichuk, Mariana ; Rambousek, Lukas ; Knuesel, Irene ; Fritschy, Jean-Marc

Abstract: Aberrant epileptic activity is detectable at early disease stages in Alzheimer's disease (AD) patients and in AD mouse models. Here, we investigated in young ArcticA mice whether AD-like pathology renders neuronal networks more susceptible to the development of acquired epilepsy induced by unilateral intrahippocampal injection of kainic acid (IHK). In this temporal lobe epilepsy model, IHK induces a status epilepticus followed after two weeks by spontaneous recurrent seizures (SRS). ArcticA mice exhibited more severe status epilepticus and early onset of SRS. This hyperexcitable phenotype was characterized in CA1 neurons by decreased synaptic strength, increased kainic acid-induced LTP and reduced frequency of spontaneous inhibitory currents. However, no difference in neurodegeneration, neuroinflammation, axonal reorganization or adult neurogenesis was observed in ArcticA mice compared to wild-type littermates following IHK-induced epileptogenesis. Neuropeptide Y (NPY) expression was reduced at baseline and its IHK-induced elevation in mossy fibres and granule cells was attenuated. However, although this alteration might underlie premature seizure onset, neutralization of soluble A species by intracerebroventricular A -specific antibody application mitigated the hyperexcitable phenotype of ArcticA mice and prevented early SRS onset. Therefore, the development of seizures at early stages of AD is mediated primarily by A species causing widespread changes in synaptic function.

DOI: https://doi.org/10.1111/ejn.13983

Section: Clinical and Translational Neuroscience (Gian Maria Maccaferri)

Contribution of early Alzheimer's Disease-related Pathophysiology to the Development of Acquired epilepsy

Tilo Gschwind[1,2], Carlos Lafourcade[1,3], Tim Gfeller[1], Mariana Zaichuk[1,2], Lukas Rambousek[4], Irene Knuesel[1,5] and Jean-Marc Fritschy[1,2]

[1]Institute of Pharmacology and Toxicology, University of Zurich, Winterthurerstrasse 190, 8057 Zurich, Switzerland

[2]Neuroscience Center Zurich, University of Zurich and ETH Zurich, 8057 Zurich, Switzerland

[3]Laboratorio de Neurociencias, Universidad de los Andes, Santiago, Chile

[4]Institute of Experimental Immunology, University of Zurich, Winterthurerstrasse 190, 8057 Zurich, Switzerland

[5]Roche Pharmaceutical Research and Early Development, NORD Discovery & Translational Area, Roche Innovation Center Basel, Grenzacherstrasse 124, Basel, Switzerland

Corresponding author: Jean-Marc Fritschy, Institute of Pharmacology and Toxicology, Winterthurerstrasse 190, 8057 Zurich, Switzerland, fritschy@pharma.uzh.ch

Running title: Epilepsy in a model of Alzheimer's disease

Number of pages: 58; Number of figures: 12; Number of Tables: 6

Number of words: Abstract: 198; Main Text 8823

Keywords: temporal lobe epilepsy, spontaneous recurrent seizures, synaptic plasticity, kainic acid, amyloid precursor protein

Abstract

Aberrant epileptic activity is detectable at early disease stages in Alzheimer's disease (AD) patients and in AD mouse models. Here, we investigated in young ArcticAβ mice whether AD-like pathology renders neuronal networks more susceptible to development of acquired epilepsy induced by unilateral intrahippocampal injection of kainic acid (IHK). In this temporal lobe epilepsy model, IHK induces a status epilepticus followed after two weeks by spontaneous recurrent seizures (SRS). ArcticAβ mice exhibited more severe status epilepticus and early onset of SRS. This hyperexcitable phenotype was characterized in CA1 neurons by decreased synaptic strength, increased kainic acid-induced LTP, and reduced frequency of spontaneous inhibitory currents. However, no difference in neurodegeneration, neuroinflammation, axonal reorganization or adult neurogenesis was observed in ArcticAβ mice compared to wildtype littermates following IHK-induced epileptogenesis. Neuropeptide Y (NPY) expression was reduced at baseline and its IHK-induced elevation in mossy fibers and granule cells was attenuated. However, although this alteration might underlie premature seizure onset, neutralization of soluble Aβ species by intracerebroventricular Aβ-specific antibody application mitigated the hyperexcitable phenotype of ArcticAβ mice and prevented early SRS onset. Therefore, development of seizures at early stages of AD is mediated primarily by Aβ species causing widespread changes in synaptic function.

Introduction

Alzheimer's disease is the most prevalent age-related dementia, characterized by progressive neuronal dysfunctions. Early stages of Alzheimer's disease and other age-related dementia are associated with aberrant network activity, including a high incidence of unprovoked epileptic seizures (Hesdorffer *et al.*, 1996; Amatniek *et al.*, 2006; Scarmeas *et al.*, 2009; Vossel *et al.*, 2013; Vossel *et al.*, 2016). Early neurochemical alterations render neuronal networks susceptible to seizure generation (Palop & Mucke, 2016). Indeed, different mouse models of Alzheimer's disease exhibit neuronal hyperactivity and even interictal spikes long before the occurrence of plaques (Busche *et al.*, 2012; Kam *et al.*, 2016). While hyperexcitability reduces seizure threshold in Alzheimer's disease-transgenic mice (Palop *et al.*, 2007; Roberson *et al.*, 2007; Westmark *et al.*, 2008; Born *et al.*, 2014), it is unknown whether it is causally related to onset of spontaneous recurrent seizures (SRS).

Alzheimer's disease and epilepsy, in particular temporal lobe epilepsy, share major pathogenic mechanisms, including neurodegeneration, synaptic dysfunction, inflammation, and altered adult neurogenesis. In mouse models of temporal lobe epilepsy, loss of parvalbumin-, calbindin-, somatostatin- and neuropeptide Y-expressing interneurons occurs in CA1 and dentate gyrus early during epileptogenesis (Bouilleret *et al.*, 2000a; Bouilleret *et al.*, 2000b; Andre *et al.*, 2001). Similarly, different mouse models of Alzheimer's disease show reduced numbers of interneurons in these regions (Ramos *et al.*, 2006; Mahar *et al.*, 2016); and functional impairments of parvalbumin-expressing interneurons were directly related to network hypersynchrony in parietal cortex (Verret *et al.*, 2012). In granule cells of the dentate gyrus, calbindin expression is disease stage-dependently reduced in mouse models and patients with Alzheimer's disease (Palop *et al.*, 2003; Stefanits *et al.*, 2014). Moreover, temporal lobe epilepsy is characterized by recurrent sprouting of mossy fiber collaterals (Buckmaster, 2012) and by ectopic expression of neuropeptide Y in dentate granule cells

(Marksteiner *et al.*, 1990; Tonder *et al.*, 1994; Vezzani *et al.*, 1999). Transgenic Alzheimer's disease mouse models revealed a similar adaptation to a hyperexcitable network, including mossy fiber sprouting onto GABAergic basket cells and hilar interneurons (Palop *et al.*, 2007). In both temporal lobe epilepsy and Alzheimer's disease, activation of innate immunity is an important pathogenic feature. For instance, in temporal lobe epilepsy, secreted cytokines render the neuronal network hyperexcitable and thereby more susceptible to seizures (Viviani *et al.*, 2003; Maroso *et al.*, 2010; Gardoni *et al.*, 2011). Likewise, amyloid β recruits microglia (Alzheimer *et al.*, 1995; Meyer-Luehmann *et al.*, 2008; Wang *et al.*, 2015) and thus triggers inflammatory cytokine release, causing various sequelae associated with Alzheimer's disease (Heneka *et al.*, 2013). Finally, neurogenesis is altered in both temporal lobe epilepsy and Alzheimer's disease. Prolonged seizure activity transiently increases precursor cell proliferation (Parent *et al.*, 1997; Jessberger *et al.*, 2005), followed by neurogenic niche destruction and impaired hippocampal neurogenesis (Kralic *et al.*, 2005; Ledergerber *et al.*, 2006; Sierra *et al.*, 2015). In Alzheimer's disease, survival of newborn neurons is impaired in mice with plaque-burden (Verret *et al.*, 2007), while in young Alzheimer's disease transgenic, accelerated development of newborn granule cells leads to impaired dendritic maturation (Sun *et al.*, 2009).

It is difficult to disentangle which Alzheimer's disease-related pathological features directly contribute to seizure development and which are by-products of a hyperexcitable environment. Therefore, we investigated temporal lobe epilepsy-related epileptogenesis in ArcticAβ mice (Knobloch *et al.*, 2007), overexpressing human amyloid precursor protein transgene containing the Swedish and Arctic mutations. The Swedish mutation shifts the balance of the amyloid precursor protein cleavage towards the beta secretase pathway, increasing the levels of carboxy-terminal fragments and ultimately β amyloid peptides. The Arctic mutation increases the aggregation tendency of Aβ without affecting the secretases.

Since neuronal dysfunctions associated with Aβ pathology occur prior to plaque deposits (Billings *et al.*, 2005; Busche *et al.*, 2012; Kam *et al.*, 2016), it is possible to separate the two phenomena. We monitored the clinical course of epileptogenesis induced by intrahippocampal injection of kainic acid (IHK) in young adult ArcticAβ mice and wildtype littermates. IHK induces a status epilepticus followed by a seizure-free 2-week latent period preceding SRS onset (Suzuki *et al.*, 1995; Bouilleret *et al.*, 1999; Riban *et al.*, 2002), allowing to causally determine the role of early Alzheimer's disease-related neurochemical alterations for epileptogenesis and development of temporal lobe epilepsy, as assessed by chronic intrahippocampal EEG recordings and immunohistochemical analysis. Finally, we tested the possible role of Aβ species and related fragments of the amyloid precursor protein (Benilova *et al.*, 2012) by inactivating them intracerebrally with a neutralizing antibody.

Materials and methods

Mice

All experiments performed for this study were carried out in accordance with the Swiss law on animal experimentation and approved by the Cantonal Veterinary Office of Zurich. ArcticAβ transgenic mice (Knobloch *et al.*, 2007) and age-matched wildtype littermates were bred at the Laboratory Animal Sciences Center of the University of Zurich. They were genotyped by PCR analysis from ear biopsies. They were housed at standard conditions (20-24℃; minimum 40% relative humidity) under a 12-hour light/dark cycle, with access to food and water *ad libitum*. Experiments were performed in males unless indicated otherwise and all group sizes are reported with the statistical analyses.

Intrahippocampal kainic acid (IHK) injection

At the age of 12-to-15-weeks, mice anaesthetized by inhalation of 2.5-3% isoflurane (Baxter) in oxygen were injected (Nanoject II, Drummond Scientific) with 70 nL kainic acid (5 mM in NaCl; Tocris biosciences) or an equivalent volume of NaCl into the right dorsal hippocampus (anteroposterior [AP] -1.8 mm, mediolateral [ML] -1.6 mm, dorsoventral [DV] -1.9 mm relative to Bregma) as described by (Bouilleret *et al.*, 2000a). For analgesia, mice were i.p. injected with 1 mg/kg buprenorphine (Temgesic®, Reckitt Benckiser AG, Switzerland) prior and after surgery. For some experiments (indicated below), a protective dose of diazepam (5 mg/kg) was administered immediately after the end of IHK injection.

Intrahippocampal retrovirus injection

Adult mice (2 months old) were anesthetized as described above. Retrovirus encoding enhanced green-fluorescent protein (eGFP; 1 µL) was bilaterally injected into the hilus of the dentate gyrus (AP -2.0 mm, ML +/- 1.5 mm, DV -2.3 mm relative to Bregma) and the tissue was collected at 21 or 42 days post injection (dpi). eGFP-encoding retrovirus was produced

133 "in house", as described in (Deprez *et al.*, 2016). HEK 293T cells were transfected with three
134 different plasmids containing the capsid (CMV-vsvg), viral proteins (CMV-gag/pol) and the
135 transgene (CAG-eGFP) under the control of the CAG promoter (including the CMV CMS
136 enhancer and chicken β-actin promoter).

137 **Antibody injection**

138 A subset of mice was intracerebroventricularly injected with purified mouse anti-Aβ antibody
139 (6E10, Aβ3–8, IgG1; Covance) or control immunoglobulin G (IgG; 4 mg/mL; kindly
140 provided by Dr. Britta Engelhardt, Theodor Kocher Institute, University of Bern) for a local
141 neutralization of soluble Aβ species (Sudduth *et al.*, 2013). A bilateral infusion (5 µL each,
142 500 nL/min, 10 min wait prior to needle retraction) into the lateral ventricles (AP -1.8 mm,
143 ML +/-2.75 mm, DV -2.5 mm relative to Bregma) was performed under general anesthesia 3
144 days prior to the IHK injection. The tissue was collected at 18 dpi (IHK injection) for
145 histological analysis.

146 **Electrode implantation for EEG**

147 For EEG recordings, mice were implanted immediately after stereotactic injection of KA
148 with a bipolar electrode into the same coordinates as the injection and a monopolar reference
149 electrode was placed into the cerebellum of the left hemisphere. Two enamel insulated
150 stainless steel wires were connected to a male connector and twisted to a bipolar electrode for
151 EEG recordings (0.125 mm inner diameter, 0.15 mm outer diameter, distance between the
152 tips = 0.4 mm; for details see (Arabadzisz *et al.*, 2005)), while two gold wires were inserted
153 into the neck muscles for EMG recordings (for details see (Palchykova *et al.*, 2010)).
154 Electrodes were connected through a board-to-board connector (M52-5050545, Harwin) and
155 fixed to the skull by a combination of Prime&Bond (Dentsply) and Tetric EvoFlow (Ivoclar
156 vivadent) while the entering electrode shaft was sheathed by Kwik-CastTM Silicone
157 Elastomer (World Precision Instruments).

EEG recordings and analysis

Mice were placed into custom-made recording cages within a Faraday cage. A custom-made vEEG system was used for continuous synchronous video and EEG recordings, consisting of a custom-made swivel, an amplifier and digitizer (AcqKnowledge MP100; Biopac Systems), infrared-switchable video cameras (Vivotek Inc., New Tapei City, Taiwan), NAS server (Synology), and a custom-made timer for synchronization (BASIC Stamp 2, Parallax Inc, Rocklin, CA, USA). EEG and EMG data was acquired at a sampling rate of 200 Hz.

Continuous video-EEG (vEEG) recordings were acquired after the injection until 18 days post injection (dpi) or once at 21 dpi. To assess the acute response to IHK, vEEG recordings of the first 4 hours were manually analyzed (open source software Polyman, EDF+). The severity of behavioral seizures was categorized according to the Racine, Pinel and Rovner scale (Table 1) (Racine, 1972; Pinel & Rovner, 1978). For each day, one hour was analyzed during the activity phase (around 1 am) and during the resting phase (around 1 pm). For seizure quantification during the chronic phase, a three-hour recording (11 am to 2 pm) was analyzed. Seizures were defined as paroxysmal events lasting longer than 20 s that were separated by intervals of at least 1 s. The average frequency and duration of spontaneous recurrent seizures (SRS) was calculated for each mouse.

Acute brain slice preparation

3-month-old mice were anesthetized with sodium pentobarbital (Nembutal®; 50 mg/kg; i.p.) and decapitated. 300 µm – thick sagittal slices were cut on a vibratome (Leica VT 1200 S) in ice-cold cutting solution and then stored in ACSF at room temperature in an interface type holding chamber for at least 1 h. Cutting solution contained (in mM) NaCl 87, KCl 2.5, $CaCl_2$ 0.5, MgCl 7, NaH_2PO_4 1.25, $NaHCO_3$ 25, glucose 10 and sucrose 75. ACSF contained (in mM) NaCl 120, KCl 3, $CaCl_2$ 2.5, $MgSO_4$ 2, NaH_2PO_4 1, $NaHCO_3$ 25, and glucose 20, and was bubbled with 95% O_2, 5% CO_2 (pH 7.4).

Field recordings

For the recording of extracellular population spikes glass microelectrodes of approx. 1.5 MΩ were filled with saline and placed near the border of CA1 stratum radiatum. Population spikes were evoked at 0.05 Hz with two pulses (50 ms apart) through a bipolar stimulating electrode positioned in CA3. A 15 min stable baseline was acquired before the application of 1µM KA for 10 min. The amplitudes of the population spikes were measured using Clampfit 10 (Molecular Devices, LCC, Sunnyvale, California, United States). To evaluate changes induced by kainic acid (KA) application, mean baseline values (mean of all amplitudes 5 min before the application of KA, i.e. 15 consecutive responses) were compared to those elicited 30 min after the washout of KA (mean of 15 consecutive responses).

Patch clamp recordings

For whole cell patch clamp recordings CA3 area was cut away. CA1 hippocampal cells were visualized with an upright microscope (Axioscope Examiner.A1, Carl Zeiss; 63x water immersion objective). Whole-cell pipettes were pulled from thin wall glass capillaries (1.5 O.D. X 1.17 I.D., Harvard Apparatus, Massachusetts, USA) using a Zeitz DMZ Puller (Martinsried, Germany). Electrode resistances in the bath were 3–6 mV. Series resistance was monitored by a –5mV step, and cells were discarded if this changed significantly (~20%). The intracellular solution consisted of (in mM) CsCl 140, HEPES 10, EGTA 10, MgATP 2, Na_3GTP 0.3, pH 7.3, 290 mOsM. Cells were clamped at a holding potential of –70 mV to register spontaneous postsynaptic currents (sPSC). Currents were recorded with a multiclamp 700B (Molecular Devices, Pennsylvania, USA), and digitized at 10 kHz using a Digidata 1550 digitizer (Molecular Devices) and Clampex 10.0 (MolecularDevices). Traces were recorded with pClamp 10 and analysis of sPSCs frequencies and amplitudes were performed with MiniAnalysis (Synaptosoft, New Jersey, USA). KA (250 nM) was added for 5 min. For each condition (i.e. before the addition of KA and in the presence of KA) traces of one-

minute duration were used for statistical analysis. The one-minute period where the effect of KA was maximal, was chosen for the statistical analysis.

RNA isolation and quantitative real-time PCR

Adult mice were anesthetized, decapitated, brains were extracted rapidly on ice and hippocampus dissected. Whole cell RNA from brain tissue was extracted using NucleoSpin RNA kit (Macherey-Nagel). cDNA was prepared using random hexamer primer (Thermo Scientific) and MuLV Reverse Transcriptase (Thermo Scientific). 1 µg of total RNA was amplified in CFX384 Touch™ Real Time PCR detection system (Biorad) using the SYBRgreen PrecisionPLUS qPCR Mastermix (Primerdesign). The relative levels of each RNA sample were calculated by the 2-ΔΔCT method using Biogazelle, qBase plus software (Livak KJ, 2001) and were normalized to that of HPRT and eEF1a1 mRNA. Each CT value used for these calculations was the mean of triplicates of the same reaction. All primers were synthesized by Eurofins genomics. Sequences of all primers are listed in Table 2.

5′-bromo-2′-deoxyuridine (BrdU) treatment

Three weeks prior BrdU treatment, adult female mice were housed together (five per cage) and bedding containing male mouse urine was introduced to the cages to induce Lee-Boot and Whitten cycle-synchronizing effects. At the age of two months, mice received two intraperitoneal injections of 90 mg/kg BrdU (Sigma-Aldrich, #B5002, dissolved in 0.9% NaCl) on two consecutive days. The tissue was collected at 1 dpi to assess cell proliferation and at 28 dpi to evaluate cell survival and cell fate.

Tissue preparation for immunohistochemistry

Tissue was collected and prepared similar to the protocol of Notter *et al.* (2014). In brief, mice were anesthetized (Nembutal®; 50 mg/kg; i.p.) and perfused intracardially with 15–20 mL ice-cold, oxygenated aCSF [containing (mM) NaCl 125, KCl 2.5, $CaCl_2$ 3.7, $MgCl_2$ 2, $NaHCO_3$ 26, NaH_2PO_4 1.25, glucose 25], pH 7.4, at a flow rate of 10–15 mL/min. The brain

was extracted and divided into 3 blocks: rostral, medial and caudal part. All three parts were immediately immersion-fixed for 3 hours in ice-cold fixative [4% paraformaldehyde dissolved in 0.15 M sodium phosphate buffer], pH 7.4, then rinsed with PBS (pH = 7.4) and cryoprotected overnight in 30% sucrose in PBS at 4°C.

The fixed tissue was cut into 70-µm (dendritic morphology) or 40-µm (rest) thick serial coronal sections using a sliding microtome and collected in ice-cold PBS. For storage, sections were transferred to a cryoprotectant solution (50 mM sodium phosphate buffer, pH 7.4, containing 15% glucose and 30% ethylene glycol; Sigma-Aldrich) and kept at -20°C.

Immunohistochemistry

Sections were washed three times in Tris buffer (50 mM Tris, 150 mM NaCl, 0.05% Triton X-100, pH 7.4) for 10 min each and incubated overnight at 4 ℃ under continuous agitation with primary antibodies (Table 3) diluted in Tris buffer containing 2% normal goat serum (NGS) and 0.2% Triton X-100. Sections were rinsed three times in Tris buffer and incubated with the secondary antibody solution (2% NGS, Tris buffer) for 30 min at room temperature with secondary antibodies raised in goat. For immunofluorescence, secondary antibodies conjugated to AlexaFluor-488 (Invitrogen) were diluted to 1:1000 and those conjugated to Cy3 or Cy5 (Jackson ImmunoResearch Laboratories) to 1:500. After washing three times in PBS, sections were mounted to gelatin-coated glass slides and cover-slipped using Fluorescence Mounting Medium (Dako). For immunoperoxidase staining, biotinylated secondary antibodies (Jackson ImmunoResearch Laboratories) were diluted 1:300 and after washing three times in Tris buffer, incubated with avidin-peroxidase-complex solution (Vectastain Elite kit, Vector Labs) at room temperature. After washing them again three times in Tris buffer, sections were stained by combining 3,3-diaminobenzidine (DAB; Sigma–Aldrich Inc.) in Tris buffer (pH 7.7) with hydrogen peroxide for 5-15 min. Sections were immediately transferred to ice-cold PBS and washed three times. Finally, sections were

mounted onto gelatinized glass slides, air-dried overnight, dehydrated through ethanol, cleared in xylene and coverslipped with resinous (Eukitt™; Sigma-Aldrich) mounting medium.

Nissl staining

The IHK-induced pattern of degeneration and the placement of EEG electrodes were determined by Nissl staining with Cresyl violet. To this end, slides with air-dried sections were dipped in the following solutions: 5 min in dH_2O, 5 min in filtered Cresyl violet solution ($C_{18}H_{15}N_3O_3$, M 321.34, Fluka BioChemika, Cat. no. 10510-54-0), 30 sec in dH_2O and cleared in 96% ethanol containing 0.5% acetic acid until the desired coloration was obtained, 5 min in isopropanol, 5 min in isopropanol:Xylene (1:2) and 4 times dehydrated in xylene for 2 min. Finally, the slides were coverslipped with Eukitt.

Experimental design and quantification

All analyses were performed by an observed blinded to the genotype and/or age of the mice. Treatment (saline versus kainic acid) was not blinded due to obvious morphological alterations induced by kainic acid.

Visual scoring and image acquisition

For visual scoring of the neurodegenerative pattern (Nissl), 3-4 sections per mouse were examined using an Axioscop 2 microscope (Carl Zeiss) with bright-field illumination and either a 10x, 20x objective or 40x oil immersion objective. All images for display were acquired with a color digital camera (AxioCam MRc5) and the corresponding software AxioVision 4.5 (Zeiss).

Densitometry analysis

Immunoperoxidase staining (CD68, NPY) intensity was assessed by densitometry analysis using the MCID software (MCID Elite 6.0, InterFocus Imaging Ltd., Cambridge, UK). First, images were digitized using a precision illuminator (Northern light Model B95, Imaging

Research Inc., Brock University, St.Catharines, Canada) and CoolSnap cf photo-camera (Photometrics, Tuscon, AZ, USA) with a Micro-Nikkor (55 mm + 12 mm) objective (Nikon Corp.). Then, the grey values were calibrated (Kodak step tablet no. 310ST607) and the intensity was measured in the different regions of interest (Fig. 1A). To correct for variations in background staining, the intensity value was normalized to the intensity of the whole section and for each mouse, the intensity of a particular area was averaged over three to four equidistant coronal sections.

Stereological analysis of macrophage-like cells

The number of F4/80+ macrophage-like cells was determined stereologically in series of randomly sampled brain sections (three to four per animal, sampling fraction 1/12) using an Axioplan 2 bright-field microscope (Carl Zeiss AG, Feldbach, Switzerland) with 20x (air, NA 0.75) objective and an integrated digital camera (MicroFIRE, Optronics AG, Goldach, Switzerland). The size of the granule cell layer and molecular layer of the dentate gyrus as well as the number of macrophage-like cells within these outlined regions (Fig. 1B) were estimated using the Mercator software (Mercator Pro rev. 7.8.2, Explora Nova, La Rochelle, France). The macrophage-like cells were counted exhaustively and together with the estimated thickness averaged per animal.

Quantification of cell proliferation and survival

BrdU+ cells in the subgranular zone and granule cell layer of the dentate gyrus were counted in four to five sections per mouse in dorsal hippocampus using the Axioscop 2 (Carl Zeiss; 40x oil-immersion lens, NA 1.3). Dorsal hippocampal volume was estimated using Mercator software (compare above).

Sholl analysis

Fluorescent Z-stacks (spaced by 0.7 µm) throughout the entire thickness of the section were acquired with a confocal microscope (LSM710) using a 40x oil immersion objective (NA,

1.4) and ZEN 2012 black edition (Carl Zeis MicroImaging GmbH, Goettingen, Germany) software. Images were analyzed with ImageJ (version 1.49o; Java 1.6.0_12 (Wayne Rusband, National Institutes of Health, USA). Sholl analysis (Sholl, 1953) (concentric circles spaced at 10 µm intervals, centered on the cell body) was used to analyze the complexity of the dendritic trees. First, neurons were traced using NeuronJ plugin (NIH ImageJ; (Meijering *et al.*, 2004)). Further Sholl analysis plugin (Anirvan Ghosh Laboratory, University of California, San Diego, La Jolla, CA, USA) was used to calculate the number of intersections between dendrites and concentric circles. For the number of intersections as a function of distance from the soma, area-under the curve (AUC) was calculated and used for further statistical analysis. Dendritic morphometry (primary dendrite length, total dendrite length) was assessed with the NeuronJ plugin. In total 14-36 cells from the groups of 5 to 8 mice per time point were quantified.

Spine density

Z-stacks for spine density morphology analysis of randomly selected eGFP-positive dendritic segments were obtained with a 40x oil immersion objective using a 2.7 digital zoom. Spines density quantification and spine type classification were performed using CellCounter (ImageJ). The length of each segment was measured and the number of spines/µm was quantified.

Statistical analysis

Data are presented as mean ± standard error of the mean (SEM). Statistical analyses for multiple group comparison were performed by a one-way or two-way ANOVA with a Bonferroni post-hoc test. An unpaired t test, two-tailed, was used to compare two groups (Prism software, GraphPad version 6). For kainic acid-induced LTP a two-way repeated measure ANOVA was performed with a Sidak´s multiple comparisons test. To compare the

distribution of spontaneous currents (inter-event interval and amplitude) a Kolmogorov–Smirnov test was used (differences were considered significant if $p<0.0001$).

335 # Results

336 ## Acquired epilepsy and increased seizure-associated mortality in ArcticAβ mice

337 To determine whether an Alzheimer's disease-like predisposition prior to detectable plaque
338 pathology renders the limbic neuronal network more vulnerable to excitotoxicity and affects
339 the development of acquired epilepsy, 3-month-old ArcticAβ mice and wildtype littermates
340 were injected intrahippocampally with kainic acid (IHK) (Fig. 2A). Upon recovery from
341 anesthesia, IHK induces a status epilepticus with occasional convulsive seizures in wildtype
342 mice. ArcticAβ mice exhibited a much more severe reaction, with numerous convulsive
343 seizures causing acute mortality. Nevertheless, the characteristic neurodegeneration pattern
344 seen 21 days post-injection (dpi) in this model (Bouilleret *et al.*, 2000a; Bouilleret *et al.*,
345 2000b), with loss of pyramidal cells in CA1 and CA3c and loss of hilar mossy cells in the
346 dentate gyrus was the same in both genotypes (Fig. 2B). The severity and region-specificity
347 of the cell loss were not different between the genotypes. IHK-induced granule cell
348 dispersion in the dentate gyrus was also similar in ArcticAβ and wildtype littermates, as
349 determined by measuring the thickness of the granule cell layer (GCL; $t_{20} = 1.13$, $P = 0.27$)
350 and the molecular layer (ML; $t_{20} = 1.4$, $P = 0.18$; unpaired two-tailed t-test) (Fig. 2C). The
351 number of invading macrophages, which was shown to correlate with the extent of granule
352 cell dispersion (Zattoni *et al.*, 2011), did not differ between genotypes (ML: $t_{20} = 1.9$, $P =$
353 0.07; GCL: $t_{20} = 0.2$, $P = 0.85$; unpaired two-tailed t-test). In line with observations about the
354 neurodegenerative pattern induced by IHK, microglial activation was not altered by the
355 ArcticAβ transgene in the injected hemisphere (Fig. 2D).

356 IHK led to the development of acquired epilepsy (onset of spontaneous recurrent seizures,
357 SRS) in both genotypes, with mice exhibiting similar seizure frequency three weeks after the
358 injection ($t_7 = 0.04$, $P = 0.97$; unpaired two-tailed t-test) (Fig. 2E). However, a fraction of
359 ArcticAβ mice unexpectedly died during the latent phase, leading to a significantly different

survival probability upon IHK ($\chi 2(1) = 13.4$, P = 0.0003; Mantel-Cox test) (Fig. 2F). Thus, Alzheimer's disease-like predisposition in 3-month-old ArcticAβ mice increases susceptibility towards IHK, possibly by altering the response to excitotoxicity and causing aberrant activity during early epileptogenesis, while having no effect on SRS frequency and associated histopathological alterations in surviving mutant mice.

Increased response to excitatory stimulation in the hippocampal network

To study the causes of differential impact of IHK-induced status epilepticus on the hippocampal neuronal network of ArcticAβ mice, we recorded field population spikes in the main hippocampal output region, CA1, in tissue slices (Fig. 3A). A current-voltage plot illustrates the significantly different slope ($P < 0.01$, $F_{(1,16)} = 9.9$) of recorded population spikes as a function of stimulus intensity in wildtype compared to ArcticAβ mice (Fig. 3B). This difference suggests that the strength of synaptic transmission in CA1 is reduced in ArcticAβ mice, which is consistent with previous findings in other AD transgenic mice (Palop *et al.*, 2007).

Kainic acid (KA) has recently been shown to induce an NMDA-independent form of long term potentiation (LTP) (Petrovic *et al.*, 2017). Similarly, we observed that a 10-min application of KA (1 µM) produces a stable potentiation of CA1 population spikes, which remained unchanged for at least 30 min after the drug had been washed out, in both wildtype (98.7 % ± 0.9 before KA to 116.7 % ± 7.4 after 30 min washout, 9 slices from n = 7 different animals) and ArcticAβ mice (101.1% ± 3,36 before KA to 177.7 % ± 26.10 after 30 min washout, 6 slices from n = 5 different animals) (Fig. 3C). The KA-induced potentiation was significantly higher in ArcticAβ mice compared to wildtype littermates (Fig. 3D) (two-way repeated measure ANOVA; significant effect of treatment 30 min after wash-in, $F_{(1,10)} = 8.6$, $P < 0.01$, and genotype, $F_{(1,10)} = 8.6$, $P < 0.05$). The latter difference was due to the stronger effect of KA in slices of ArcticAβ mice (Sidak´s multiple comparison post-hoc test).

Although not significant, we observed a tendency towards reduced paired pulse ratio after KA in ArcticAβ mice (Fig. 3E), suggesting some degree of presynaptic involvement in their enhanced response to KA.

Impairment of the inhibitory circuit in CA1

In order to examine the response of the inhibitory CA1 microcircuit to KA application without interfering pharmacologically with KA receptors, we isolated the CA1 region from CA3 by cutting out the latter with a scalpel and performed whole cell patch clamp recordings of CA1 pyramidal cells (Fig. 4A). To measure predominantly GABA currents, we used an intracellular solution consisting of a high Cl^- concentration (see *Materials and Methods*). Most spontaneous events recorded were inhibitory (sIPSCs), as the addition of ionotropic glutamate receptor blockers did not change the frequency of baseline activity, whereas the application of 20 µM bicuculline blocked most spontaneous activity (data not shown). Therefore, we will henceforth refer to the recorded spontaneous events as sIPSCs.

Hippocampal network hyperactivity is an early symptom in AD (Palop & Mucke, 2016), and an increase in inhibitory activity in the dentate gyrus of $hAPP_{FAD}$ mice has been postulated as a compensatory mechanism (Palop *et al.*, 2007). We observed no difference in baseline frequency of sIPSCs between wildtype and ArcticAβ mice in CA1 cells, and only a small change in their amplitude. However, the application of 250 nM KA significantly diminished the frequency of events in the mutant, but revealed no genotype difference in their amplitude (Fig. 4B). In slices from wildtype mice, KA increased the frequency of sIPSCs (data not shown), as shown previously (Fisher & Alger, 1984). In line with this finding, we observed that the clustering of these events before and after KA application differed between genotypes. To quantify this phenomenon, clusters of activity were defined as groups of sIPSCs occurring within less than 100 ms from each other, and binned them into four main groups, containing up to 3 events, 4-6 events, 7-9 events or >10 events (Fig. 4C). ArcticAβ

410 mice showed more clusters with a higher number of events during baseline, which
411 disappeared in the presence of KA, whereas the opposite occurred for wildtype mice.

412 **Severe status epilepticus and early seizure onset during epileptogenesis**

413 Having observed an increased mortality in ArcticAβ mice during early stages of
414 epileptogenesis (Fig. 2F), we used video-EEG (vEEG) monitoring to determine whether
415 ArcticAβ mice suffer from more severe seizures during status epilepticus and die from
416 convulsive seizures during the latent phase (Fig. 5A). During the first four hours of status
417 epilepticus, ArcticAβ mice had more severe behavioral seizures (stage 6-7 of the Racine-
418 Pinel-Rovner scale; Table 1) than wildtype littermates even after reducing the dose of KA by
419 half to 2.5 mM (Fig. 5B; left panel). Tonic-clonic seizures (stage 8) were only observed in
420 ArcticAβ mice (Fig. 2F), and were lethal in some cases. However, neither the number (Fig.
421 5C) nor the duration (Fig. 5D) of seizures differed between genotypes. Mortality was a major
422 confounding factor in our study, because it implied that ArcticAβ mice that survived the
423 status epilepticus might have only mild lesions induced by KA. Therefore, we decided to
424 administer all mice a protective dose of diazepam (5 mg/kg) immediately after the end of
425 IHK injection (Fig. 5A). As expected, diazepam treatment strongly reduced seizure severity
426 (stage 2-3 of the Racine-Pinel-Rovner scale; Fig. 5B; right panel) and frequency (convulsive:
427 $F_1 = 52.94$, $P < 0.0001$; non-convulsive: $F_1 = 6.16$, $P = 0.025$; Fig. 4C), while having no
428 effect on seizure duration (Fig. 4D). Moreover, diazepam treatment after IHK injection
429 averted status epilepticus-associated mortality, but not mortality occurring during the latent
430 phase (Fig. 5F). Thus, increased susceptibility to severe behavioral seizures can not only be
431 evoked by a proconvulsant, but also by spontaneous aberrant network activity in a later stage
432 of epileptogenesis.

433 To determine whether abnormal EEG activity during early epileptogenesis is associated with
434 mortality during the latent phase, we acquired continuous vEEG recordings during the

progress of epileptogenesis. As reported (Riban *et al.*, 2002; Arabadzisz *et al.*, 2005), wildtype mice exhibit initially low voltage spikes or sharp waves (200-800 μV, 1-3 Hz), whereas SRS (800-1500 μV, 3-5 Hz, duration > 20 s) appear two weeks after IHK injection (Fig. 5E). ArcticAβ mice, however, showed a mixture of low voltage spikes and sharp waves (200-800 μV, 1-3 Hz) up to 3-4 dpi, with a subsequent early onset of SRS-like events (800-1500 μV, 3-5 Hz, duration 10 - 20 s) at 4-5 dpi (Fig. 5E). These early short SRS were progressively replaced by regular SRS (duration > 20 s) from 12 dpi on. Interestingly, mortality of ArcticAβ mice during the latent phase (Fig. 4F) was associated with early onset of SRS at 3 dpi (Fig. 5E). Thus, ArcticAβ mice are more susceptible to the development of seizures, even when they are "protected" with diazepam during the IHK-induced status epilepticus. These findings suggest that early onset of SRS in ArcticAβ mice is due either to a missing anticonvulsive protection or a premature proconvulsive environment during the otherwise seizure-free latent period.

Gradual progression of neurodegeneration and microgliosis during epileptogenesis

Neurodegeneration and inflammation play an important role in the pathogenesis of both AD (Heppner *et al.*, 2015) and TLE (Vezzani & Viviani, 2015). To test whether the hyperexcitable phenotype observed in ArcticAβ mice accelerates the development of a pro-epileptogenic lesion, we determined the course of neurodegeneration (data not shown) and microglial activation (CD68 immunoreactivity) in the dorsal hippocampus at different time-points (1, 3, 6, 14 dpi) of epileptogenesis (Fig. 6 and Table 4). Cresyl violet staining in adjacent sections was used to assess the neurodegenerative pattern. As expected (Bouilleret *et al.*, 1999), hilar cells in the dentate gyrus were lost and pyramidal cells in CA1 became pyknotic within 24 h. During the progression of epileptogenesis, pyramidal cells in CA1 and in CA3c gradually degenerated, starting at 3 dpi up to an almost complete disappearance at

14 dpi. Dentate gyrus GC dispersion was clearly evident at 14 dpi (data not shown) and progressed further at 21 dpi (Fig. 2B). Both genotypes showed a gradual increase of CD68-IR (a marker of microglia activation) compared to control animals over a two-week period in the ipsilateral hippocampus (in all layers of CA1, the stratum lacunosum moleculare, CA3c and the strati pyramidale and radium of CA3 a,b; Fig. 6 and Table 4). Microgliosis peaked between 1 and 6 dpi in the hilus and the stratum lucidum, while being very low in the molecular layer and GC layer. Interestingly, ArcticAβ mice exhibited a less enhanced CD68-IR compared to wildtype mice in the stratum oriens of CA3a,b at 1 dpi, and at 6 dpi in the hilus of the ipsilateral hippocampus (Table 4). The contralateral hemisphere showed increased CD68-IR except in stratum pyramidale of CA1, the stratum lacunosum-moleculare, or CA3c (Fig. 6B).

In addition, tissue of ArcticAβ mice that died during status epilepticus (~45 min after injection; Fig. 2F) was compared to a group of wildtype littermates perfused 45 min post-injection ("SE group"). We evaluated whether these ArcticAβ mice belonged to a subgroup with particularly pronounced sequelae associated with the AD pathology (including ectopic cell death and aggravated inflammation). Cresyl violet (data not shown) and CD68-IR (Fig. 6B) revealed no difference between genotypes or between hemispheres suggesting that neither an AD-like predisposition nor the IHK injection affected cellular integrity or microglial activation during early status epilepticus. Thus, the general progression of neurodegeneration and microgliosis does not reflect increased vulnerability to aberrant excitation and does not predict early onset of SRS in AD transgenic mice during IHK-induced epileptogenesis.

Examining the course of epileptogenesis revealed an impaired upregulation of neuropeptide Y in ArcticAβ mice

Neuropeptide Y has anticonvulsive properties and is immediately upregulated in mossy fibers after increased excitation (Guo *et al.*, 2002; Tu *et al.*, 2005; Gotzsche *et al.*, 2012). Reduced NPY expression has been reported in patients (Beal *et al.*, 1986; Minthon *et al.*, 1990) and animal models of AD (Ramos *et al.*, 2006). Therefore, we determined whether AD-like pathology in 3-month-old ArcticAβ mice interferes with seizure-induced upregulation of NPY in the dorsal hippocampus at different time-points (1, 3, 6, 14 dpi) of epileptogenesis.

In contrast, epileptogenesis-associated increase in neuropeptide Y expression was altered in ArcticAβ mice (Fig. 7 and Table 5). In wildtype mice, neuropeptide Y-IR was increased bilaterally, reaching significance in a region- and time-dependent manner across the various regions of the hippocampal formation (Fig. 7B). The increase was seen in both the granule cells and mossy fibers, as well as in interneurons contralaterally in CA1 and CA3. In comparison, ArcticAβ mice only displayed a moderate increase of neuropeptide Y-IR at 1-3 dpi ipsilaterally and at 1-14 dpi contralaterally in the hilus and CA3c (Fig. 7 and Table 5). In the so-called SE group, there was no difference between wildtype mice perfused 45 min after injection and ArcticAβ mice that died due to a severe status epilepticus (Fig. 7B). Thus, while status epilepticus provokes a transient increase in NPY in dorsal hippocampus of wildtype mice, peaking after 24 hours and gradually declining over two weeks, this mechanism seems to be partially impaired in ArcticAβ mice. In line with these findings, reduced neuropeptide Y expression has been reported in patients (Beal *et al.*, 1986; Minthon *et al.*, 1990) and animal models of Alzheimer's disease (Ramos *et al.*, 2006).

Impairment of NPY expression as an early sequelae of AD pathology

Interestingly, when we determined the hippocampal expression of markers involved in NPY signaling, ArcticAβ mice showed a significantly reduced expression of NPY at both three and

nine months of age ($F_{(1,16)}$ = 4.7, P = 0.047; two-way ANOVA, Bonferroni post-hoc test; Fig. 8A). The NPY receptor 1 (YR1) expression was not affected ($F_{(1,16)}$ = 1.12, P = 0.3064; two-way ANOVA; Fig. 8B), but ArcticAβ mice exhibited an increase in YR2 expression at nine months ($F_{(1,16)}$ = 1.12, P = 0.3064; two-way ANOVA; Fig. 8C) and a reduced YR5 expression at three months of age ($F_{(1,16)}$ = 1.12, P = 0.3064; two-way ANOVA; Fig. 8D).

Previous studies in hAPP-J20 mice reported sprouting of NPY+ axons in the molecular layer, ectopic expression of NPY in mossy fibers, increased recurrent sprouting of mossy fiber collaterals (Timm staining or zinc transporter ZnT3-IR) and depletion of calbindin (CB) in GC (Palop *et al.*, 2003; Palop *et al.*, 2007). Increased levels of neuropeptides, most notably NPY in areas with high plaque burden, might reflect an attempt to counteract degeneration (Diez *et al.*, 2003). Therefore, we determined whether NPY, ZnT3 and CB were changed in naive ArcticAβ mice before (three months) or after (nine months) occurrence of Aβ plaques (Fig. 8E-G). Compared to wildtype littermates (n = 6-8 / time point) no difference in NPY-IR was observed in the hilus and molecular layer of the dentate gyrus at either time-point (Fig. 8E). Similarly, visual assessment of ZnT3-IR (Fig. 8F) and CB-IR (Fig. 8G) in GCs and in CA3 revealed no difference between genotypes. Together, these observations suggest that, albeit NPY and YR5 gene expression is reduced in ArcticAβ mice prior to occurrence of Aβ plaques, NPY-IR remains unaffected in 9-month-old mutants.

Plaque pathology in Alzheimer's disease and associated inflammatory response

To confirm this conclusion, we verified in 3- and 9-month-old transgenic mice that the occurrence of plaques, microglial activation and expression of inflammatory markers occur as reported in the literature (Fig. 9). While intracellular Aβ deposits have been reported in 3-month-old ArcticAβ mice (Knobloch *et al.*, 2007), plaques, positive for 6E10 antibody, appear between seven and nine months of age with a progressive increase thereafter (Fig. 9A). As seen by CD68-staining, Aβ plaques are surrounded by reactive microglia, but up to

the age of nine months there is no general microglia activation (Fig. 9B-C and Table 6). qPCR analysis of inflammatory cytokines in hippocampal samples revealed a decreased expression of IL-10 over time in both genotypes (two-way ANOVA, $F_{(1,16)} = 11$, $P = 0.004$; Fig. 9D) and a different expression of IL-1β between genotypes (two-way ANOVA, $F_{(1,16)} = 4.7$, $P = 0.047$; Fig. 9E). No difference was detected in TNFα expression between wildtype and ArcticAβ mice at the age of 3 and 9 months ($F_{(1,16)} = 1.19$, $P = 0.291$; two-way ANOVA; Fig. 9F), whereas the expression of triggering receptor expressed on myeloid cells 2 (Trem2) - a cell surface receptor expressed on microglia cells that was proposed to be important for phagocytosis and removal of apoptotic cells and β-amyloid without being accompanied by inflammation (Colonna & Wang, 2016) - was increased concomitant with the appearance of Aβ plaques in 9-month-old ArcticAβ mice ($F_{(1,16)} = 6.8$, $P = 0.02$; two-way ANOVA, Bonferroni post-hoc test; Fig. 9G).

Genotype-specific differences in hippocampal adult neurogenesis

A large body of literature suggests a direct link between aberrant excitability and adult neurogenesis (Jessberger *et al.*, 2005; Kralic *et al.*, 2005; Ledergerber *et al.*, 2006; Song *et al.*, 2012; Sierra *et al.*, 2015). We explored the hypothesis that ArcticAβ mice, like other AD-transgenic mice (Sun *et al.*, 2009), show impaired neurogenesis, which has been reported to exacerbate KA-induced status epilepticus (Iyengar *et al.*, 2015). In order to assess proliferation and survival rate of newborn cells in the subgranular zone (SGZ) of the dentate gyrus, mice were injected with BrdU and tissue was collected at 1 and 28 dpi to assess proliferation and cell survival, respectively (Fig. 10A). At 1 dpi, ArcticAβ mice showed significantly more BrdU+ cells in the SGZ compared to wildtype littermates (14039 ± 1243 cells/mm^3, N = 8; 10415 ± 728 cells/mm^3, N = 8; data shown as mean ± SEM; $P = 0.03$, paired, two-tailed Student's t-test), while there was no difference between genotypes at 28 dpi (ArcticAβ: 2663 ± 261.8 cells/mm^3, N = 9; wild-type: 3384 ± 491 cells/mm^3, N = 9; data

557 shown as mean ± SEM; P = 0.21, paired, two-tailed Student's t-test) (Fig. 10B). To determine
558 the fate of $BrdU^+$ cells at 28 dpi, we used neuronal (NeuN) or astroglial (GFAP) markers. In
559 both genotypes a similar proportion of neuronal (NeuN/BrdU; wildtype: 89.4% ± 2.6%, N =
560 9; ArcticAβ: 91.5% ± 3.5%, N=7) and astroglial (GFAP/BrdU; wildtype: 7.5% ± 2.5%, N =
561 9; ArcticAβ: 5.9% ± 3.1%, N=7) progenitors were observed. Further, we examined the
562 morphological development of immature (21 dpi) and mature (42 dpi) newborn neurons
563 infected with a retrovirus expressing eGFP (Fig. 10C). Sholl analysis of adult-born GC at 21
564 and 42 dpi revealed a tendency towards a reduced dendritic arborization between genotypes
565 (Fig. 10D). However, further away from the soma, starting from 150µm, this difference was
566 statistically significant at both 21 dpi (wildtype: 197.4 ± 31, N = 27; ArcticAβ at 21 dpi: 70 ±
567 23, N = 14; P = 0.0094) and 42 dpi (wildtype: 359 ± 25, N=36; ArcticAβ: 258 ± 34, N=17; P
568 = 0.0221; data displayed as area under the curve (AUC), mean ± SEM, paired, two-tailed
569 Student's t-test). Moreover, dendritic spine density was assessed and spines were classified in
570 three subgroups (Fig. 10E). Overall spine density was significantly reduced in ArcticAβ mice
571 at 21 dpi, with a specific reduction in thin spines. At 42 dpi, adult-born GC of ArcticAβ mice
572 had significantly fewer stubby spines, while overall spine density was normalized. At both
573 time-points, the proportion of spine types did not differ between animals. Although ArcticAβ
574 mice had increased cell proliferation, the survival of both neuronal and glial progenitors
575 seems to be reduced. Together with the reduced spine density in adult-born GC, these
576 findings point towards a slight impairment of neurogenesis in 3-month-old ArcticAβ mice.

577 **Epileptogenesis-associated changes in hippocampal adult neurogenesis**

578 Neuronal stem cells divide into reactive astrocytes after IHK-induced status epilepticus,
579 which ultimately leads to depletion of the neuronal stem cell pool and thereby, long-term
580 impairment of adult neurogenesis (Sierra *et al.*, 2015). To evaluate whether the alterations in
581 proliferation and survival of progenitor cells in ArcticAβ mice accelerates the disruption of

582 neurogenesis during epileptogenesis, we analyzed DCX^+ neuronal precursor cells at different
583 time points (1, 3 , 6, 14 dpi) after IHK-induced status epilepticus (Fig. 11). DCX-IR
584 decreased over time in both genotypes (two-way ANOVA, $F_{(4, 40)} = 38.9$, $P < 0.0001$), and at
585 a similar rate (Fig. 11A), as previously described in wildtype mice (Ledergerber *et al.*, 2006).
586 In controls, DCX^+ cells, which are located close to the SGZ, send their dendrites into the
587 molecular layer (Fig. 11A). Ipsilaterally, DCX+ processes disappear within 1 dpi, followed
588 by a gradual disappearance of most cell bodies until 14 dpi. Contralaterally, DCX-IR
589 remained unchanged until 6 dpi, and increased at 14 dpi. However, there was no difference
590 between ArcticAβ mice and wildtype littermates. Similarly, both genotypes exhibited a
591 comparable number of ectopic cells in the hilus (two-way ANOVA, $F_{(11, 96)} = 1.20$, $P <$
592 0.2964; Fig. 11B). In addition, ArcticAβ mice that died during status epilepticus did not
593 differ from wiltype mice at 45 min post-injection with regard to DCX-IR or number of
594 ectopic cells in the ipsilateral hilus (Fig. 11B). Taken together, the decline of neuronal
595 progenitors after IHK-induced epileptogenesis follows a similar course in both genotypes.

596 **Soluble Aβ species contribute to the early onset of SRS during IHK-induced**
597 **epileptogenesis**

598 Given that 3-month-old ArcticAβ mice do not show any plaques while constitutively
599 overexpressing Aβ (Knobloch *et al.*, 2007), we aimed to determine whether a clearance of
600 soluble Aβ species and other fragments of the amyloid precursor protein might prevent the
601 early onset of SRS in these mice. Three days prior to the IHK-induced status epilepticus, a
602 mouse anti-Aβ antibody (6E10) or a control IgG were bilaterally injected into the lateral
603 ventricles on the anterio-posterior plane of the IHK-injection side (Fig. 12A). Mice were then
604 subjected to continuous vEEG during the next three weeks and seizure-like events were
605 analyzed. Interestingly, injection of Aβ antibody alleviated the epileptic phenotype in
606 comparison to an IgG injection in ArcticAβ mice (Fig. 12B). While three out of four IgG-

injected ArcticAβ mice exhibited regular SRS from 3-4 dpi, as shown above (Fig. 4E), and one died from convulsive seizures at 12 dpi, the four mice treated with Aβ antibody only had a few SRS-like events and did not develop SRS during the first 14 days post-IHK. In addition, several mice injected with IgG showed tonic-clonic seizures whereas only one of the ArcticAβ mice injected with Aβ antibody had a convulsive seizure. One IgG-injected animal exhibited multiple short clusters of spikes that were considered to be SRS-like events (B1 in Fig. 12B). In contrast, one mice injected with Aβ antibody had a transient phenotype, with only two short SRS-like events at 3 dpi, while otherwise the EEG pattern was characterized by short clusters of spikes (B2 in Fig. 12B). Noteworthy, this mouse (C3 in Fig. 12C), like the others, revealed the normal neurodegenerative pattern of the IHK-model (Bouilleret *et al.*, 1999): degeneration of pyramidal cells in CA1 and CA3c, as well as of hilar cells in the dentate gyrus (Fig. 12C). In the eight mice administered with IgG or Aβ antibodies, no GC dispersion was seen, suggesting a potential interference between the two processes. Taken together, antibody-mediated neutralization of soluble Aβ species and other fragments of the amyloid precursor protein prevented the occurrence of SRS during the latent phase in 3-month-old ArcticAβ mice, suggesting that Aβ overexpression promotes epileptogenesis in these mice.

Discussion

This study was designed to determine whether neuronal hyperactivity, which is characteristic of several mouse models of familial AD, might lead to the generation of SRS. To this end, we used the IHK-model of temporal lobe epilepsy to determine whether transgenic expression of mutant APP in Arctic Aβ mice facilitates the progression of epilepsy and seizure onset. The results indicate that ArcticAβ mice exhibit increased susceptibility towards KA-induced hyperexcitability long before the stage of plaque formation. In these mice, the strength of GABAergic inhibition in the CA1 region is reduced and LTP is facilitated. Hyperexcitability in ArcticAβ mice leads to lethal convulsions during status epilepticus, which can be prevented by diazepam. In addition, it leads to the premature onset of SRS, and in some mice, to lethal convulsive seizures during the first three weeks post-IHK. This increased seizure susceptibility does not correlate with aggravated neurodegeneration, altered synaptic reorganization, immune responses or adult neurogenesis, but is paralleled by a reduced gene expression of NPY – a neuropeptide with anti-convulsant properties – and, most strikingly, reduced upregulation of NPY-IR in granule cells of the dentate gyrus. Importantly, hyperexcitability could be reversed upon neutralization of soluble Aβ species and other fragments of the amyloid precursor protein, arguing against constitutive adaptation mechanisms and in favor of a direct effect of Aβ species on synaptic, in particular GABAergic, transmission in the hippocampal formation. Therefore, our results are consistent with the hypothesis that seizures occurring in AD-patients, especially at early disease stages, are due to synaptic and neuronal effects of Aβ species.

Hyperexcitability and epileptogenesis in AD mouse models

AD is associated with network abnormalities, characterized by hypersynchrony and altered oscillatory activity that precede clinical disease onset (Palop & Mucke, 2016). Epileptiform activity has been reported in AD patients, in particular at early stages (Amatniek *et al.*, 2006;

650 Scarmeas *et al.*, 2009; Vossel *et al.*, 2013; Vossel *et al.*, 2016) and with a higher incidence
651 during sleep (Horvath *et al.*, 2017; Lam *et al.*, 2017). Recent studies confirmed that
652 hyperexcitability in AD mouse models appears prior to plaque and tangle pathology. For
653 example, 25% CA1 pyramidal cells are hyperactive in mice overexpressing human APP with
654 a Swedish mutation and mutant human presenilin 1 (APP/PS1) already at an age of 1.5
655 months (Busche *et al.*, 2012). This neuronal dysfunction was rescued by acute treatment with
656 a γ-secretase inhibitor and neuronal hyperexcitability was induced in wildtype mice by
657 applying soluble Aβ. Although which cell types are most vulnerable and therefore first
658 affected by Aβ is not fully clarified, interneurons are among the earliest cells affected.
659 Axonal loss of SOM+ interneurons in CA1 was reported in APP/PS1 mice at pre-plaque
660 stage, and at later stages correlating with proximity to Aβ plaques (Schmid *et al.*, 2016),
661 suggesting that GABAergic boutons are affected early by soluble Aβ species. In line with
662 these findings, we found in young ArcticAβ mice that decreased synaptic strength and
663 increased KA-induced LTP are associated with changes in sIPSCs in CA1 pyramidal cells.
664 Unlike previous studies using mice overexpressing human APP with a Swedish mutation
665 (hAPP-J20) at plaque-bearing stage (Palop *et al.*, 2007), we did not find any increase in
666 inhibitory activity at baseline. As suggested by (Palop *et al.*, 2007), increased inhibitory
667 activity might be a compensatory response to an hyperexcitable phenotype. Such
668 compensatory mechanism might explain clustered sIPSCs at baseline in ArcticAβ mice (Fig.
669 5). Ectopic expression of NPY and sprouting of GABAergic axons has been reported in
670 different AD mouse models (Chin *et al.*, 2004; Palop *et al.*, 2007; Roberson *et al.*, 2007). Our
671 results indicate that these effects differ between models, especially in the timing of their
672 appearance. Nevertheless, plaque-independent Aβ toxicity appears as a predominant feature
673 altering local inhibitory circuits and increasing network excitability during early stages of the
674 AD pathogenesis. Another factor that could have played a major role to explain the

hyperexcitability phenotype of Arctic Aβ mice, as well as early SRS onset, are potential differences in adult neurogenesis (Sun *et al.*, 2009; Sierra *et al.*, 2015). However, our results reveals only minor genotype-dependent changes in adult neurogenesis, which are not exacerbated upon IHK, making this hypothesis unlikely in our view.

Increased susceptibility to induced seizures have been reported in different mouse models of AD (Palop *et al.*, 2007; Roberson *et al.*, 2007; Roberson *et al.*, 2011; Sanchez *et al.*, 2012; Verret *et al.*, 2012; Kam *et al.*, 2016). AD transgenic mice show age-dependent, and therefore disease-stage-dependent, occurrence of SRS with hippocampal origin (Palop *et al.*, 2007; Minkeviciene *et al.*, 2009; Kam *et al.*, 2016). In our model, it is unclear which mechanisms underlie the development of SRS. We have shown previously that the latent period can be massively curtailed in mutant mice lacking lymphocytes (RAG1-knockout), which exhibit SRS within 24 h of IHK (Zattoni *et al.*, 2011; Deprez *et al.*, 2016). Our present results indicate a key role for soluble Aβ species, but the reduced overexpression of NPY in mutant mice compared to their wildtype littermates might also be an important contributing factor, along with the differential regulation of cytokines seen in our qPCR analysis.

The role of NPY during epileptogenesis

A body of literature examined the effect of NPY on modulating excitatory transmission and its role during different stages of epileptogenesis (Baraban, 2002; El Bahh *et al.*, 2005). Erickson *et al.* (1996) reported that NPY-deficient mice are more susceptible to seizures induced by the GABAergic antagonist pentylenetetrazole (PTZ). Moreover, status epilepticus induced by repeated intraperitoneal injection of low dose kainic acid led to convulsive seizures in both genotypes at a similar concentration and within the same latency, but being lethal for 90% NPY-deficient mice compared to 22% wildtype littermates (Baraban *et al.*, 1997). Similarly, Y5R-deficient mice are more susceptible to KA, having more severe seizures and increased mortality (Marsh *et al.*, 1999). Here, we found a similar phenotype

after IHK in young ArcticAβ mice accompanied by weaker expression of NPY and Y5R at the age of injection (Fig. 6). In contrast, NPY application (Woldbye *et al.*, 1996; Baraban *et al.*, 1997; Woldbye *et al.*, 1997; Vezzani *et al.*, 1999) or hippocampal overexpression of NPY and Y2R or Y5R using rAAV vectors (Richichi *et al.*, 2004; Sorensen *et al.*, 2009; Woldbye *et al.*, 2010; Gotzsche *et al.*, 2012) were shown to have an alleviating effect on electrically or chemically induced acute seizures. In particular, seizures of higher severity and seizure-associated death were reduced upon activation of NPY signaling, while mild seizures remained unchanged. We likewise found no difference in the latency, number or duration of non-convulsive seizures in ArcticAβ mice during IHK-induced status epilepticus (Fig. 4). Moreover, at nine months of age, hippocampal Y2R expression is increased in ArcticAβ mice, similar to plaque-bearing hAPP-J20 mice (Palop *et al.*, 2007), suggesting a compensatory mechanism after months of increased excitability.

Although, the similarities between NPY-deficient animals and ArcticAβ mice are compelling, additional experiments are needed to evaluate if the decrease in NPY expression is directly responsible for the hyperexcitable phenotype of the AD model. To this end, it would be interesting to test whether neutralization of soluble Aβ species (e.g., with the 6E10 antibody) would restore NPY expression and signaling in ArcticAβ mice, and thereby ameliorate the excitability in vivo and in slices.

The role of inflammation during epileptogenesis

Perhaps the least expected finding of this study is that inflammation that accompanies neurodegeneration in the dorsal hippocampus after IHK was not more severe in ArticAβ mice, despite on-going stimulation of innate immunity by increased Aβ species and their accumulation in the brain (Knobloch *et al.*, 2007). In our previous work in RAG1-KO mice (Zattoni *et al.*, 2011), we showed that in the absence of adaptive immunity by T and B lymphocytes, IHK causes a stimulation of innate immunity mediated by neutrophils, leading

to extensive neurodegeneration in CA1-CA3 and eventually complete atrophy of the injected hippocampus. We also observed that this phenotype is accompanied by a dramatic shortening of the seizure-free latent phase that follows IHK, with RAG1-KO mice exhibiting SRS at 1-2 dpi (Zattoni *et al.*, 2011). Therefore, the disrupted balance between adaptive and innate immunity induces a condition in the brain of IHK-treated mice that favors SRS onset, presumably mediated by inflammation-related secreted or blood-born factors. Our present results show that the AD-like predisposition in ArticAβ mice also induces a condition that favors the occurrence of SRS during the latent phase, which is due, at least in large part to Aβ overexpression in the brain, and which does not stimulate further inflammatory mechanisms that would aggravate neurodegeneration. Both studies relativize the importance of neuronal circuit reorganization that takes place during the latent phase for SRS onset. Rather, they favor the view that the latent phase is seizure-free because of unknown protective mechanisms preventing seizure onset. These mechanisms can be overruled by immune factors or by hyperexcitability.

Therefore, despite the fact that temporal lobe epilepsy and AD share common pathogenic mechanisms and exhibit comparable alterations in inhibitory neuronal networks in the hippocampal formation, as outlined in the Introduction, there appears to be little cross-over between the two disease conditions. In AD patients, like in Artic Aβ mice subject to IHK, epileptogenic activity and unprovoked seizures are most likely related to toxic Aβ species affecting synaptic transmission and favoring a state of chronic hyperexcitability. Unravelling the exact mechanisms by which these Aβ species affect synaptic GABAergic transmission in AD and in Artic Aβ mice, and in particular, whether this alterations involves NPY signaling, will contribute to better understand the prevalence of epileptic seizures in AD.

Acknowledgements

We thank Dr. Mario Merlini for the 6E10 antibody and Dr. Tatjana Haenggi and Cornelia Schwerdel for mouse genotyping. This work was supported by the Swiss National Science Foundation (grant 144199 to JMF).

Author's contributions

All IHK experiments and data analysis were carried out by TGs and TGe. Electrophysiology experiments were performed by CL and TGs. BrdU and eGFP experiments were carried out by MZ. Histology and qPCR experiments in naïve mice were conducted by TGs and LR. TGs and JMF wrote the manuscript. JMF and IK planned the study, supervised the experiments and data analysis, and obtained funding. All authors read and commented on the manuscript.

Competing financial interests

The authors declare no competing financial interests.

Data Availability

Data are available upon request to the corresponding author.

Abbreviations

DAB 3,3-diaminobenzidine

BrdU 5′-bromo-2′-deoxyuridine

AD Alzheimer's disease

AUC area under the curve

CB calbindin

dpi days post injection

GCL granule cell layer

HL hilus

IgG	immunoglobulin G
icv	intracerebroventricularly
IHK	intrahippocampal injection of kainic acid
KA	kainic acid
LTP	long term potentiation
ML	molecular layer
NPY	Neuropeptide Y
NGS	normal goat serum
PTZ	pentylenetetrazole
sIPSCs	spontaneous inhibitory postsynaptic currents
sPSC	spontaneous postsynaptic currents
SRS	spontaneous recurrent seizures
SEM	standard error of the mean
SLM	stratum lacunosum moleculare
SO	stratum oriens
SP	stratum pyramidale
SR	stratum radiatum
SGZ	subgranular zone
Trem2	triggering receptor expressed on myeloid cells 2
vEEG	video-EEG

References

Alzheimer, A., Stelzmann, R.A., Schnitzlein, H.N. & Murtagh, F.R. (1995) An English translation of Alzheimer's 1907 paper, "Uber eine eigenartige Erkankung der Hirnrinde". *Clin Anat*, **8**, 429-431.

Amatniek, J.C., Hauser, W.A., DelCastillo-Castaneda, C., Jacobs, D.M., Marder, K., Bell, K., Albert, M., Brandt, J. & Stern, Y. (2006) Incidence and predictors of seizures in patients with Alzheimer's disease. *Epilepsia*, **47**, 867-872.

Andre, V., Marescaux, C., Nehlig, A. & Fritschy, J.M. (2001) Alterations of hippocampal GAbaergic system contribute to development of spontaneous recurrent seizures in the rat lithium-pilocarpine model of temporal lobe epilepsy. *Hippocampus*, **11**, 452-468.

Arabadzisz, D., Antal, K., Parpan, F., Emri, Z. & Fritschy, J.M. (2005) Epileptogenesis and chronic seizures in a mouse model of temporal lobe epilepsy are associated with distinct EEG patterns and selective neurochemical alterations in the contralateral hippocampus. *Exp Neurol*, **194**, 76-90.

Baraban, S.C. (2002) Antiepileptic actions of neuropeptide Y in the mouse hippocampus require Y5 receptors. *Epilepsia*, **43**, 9-13.

Baraban, S.C., Hollopeter, G., Erickson, J.C., Schwartzkroin, P.A. & Palmiter, R.D. (1997) Knock-out mice reveal a critical antiepileptic role for neuropeptide Y. *J Neurosci*, **17**, 8927-8936.

817 Beal, M.F., Mazurek, M.F., Chattha, G.K., Svendsen, C.N., Bird, E.D. & Martin, J.B. (1986)
818 Neuropeptide Y immunoreactivity is reduced in cerebral cortex in Alzheimer's disease. *Ann*
819 *Neurol*, **20**, 282-288.
820
821 Benilova, I., Karran, E. & De Strooper, B. (2012) The toxic Aβ oligomer and Alzheimer's
822 disease: an emperor in need of clothes. *Nat Neurosci.*, **15**, 349-357.
823
824 Billings, L.M., Oddo, S., Green, K.N., McGaugh, J.L. & LaFerla, F.M. (2005) Intraneuronal
825 Abeta causes the onset of early Alzheimer's disease-related cognitive deficits in transgenic
826 mice. *Neuron*, **45**, 675-688.
827
828 Born, H.A., Kim, J.Y., Savjani, R.R., Das, P., Dabaghian, Y.A., Guo, Q., Yoo, J.W., Schuler,
829 D.R., Cirrito, J.R., Zheng, H., Golde, T.E., Noebels, J.L. & Jankowsky, J.L. (2014) Genetic
830 suppression of transgenic APP rescues Hypersynchronous network activity in a mouse
831 model of Alzeimer's disease. *J Neurosci*, **34**, 3826-3840.
832
833 Bouilleret, V., Loup, F., Kiener, T., Marescaux, C. & Fritschy, J.M. (2000a) Early loss of
834 interneurons and delayed subunit-specific changes in GABA(A)-receptor expression in a
835 mouse model of mesial temporal lobe epilepsy. *Hippocampus*, **10**, 305-324.
836
837 Bouilleret, V., Ridoux, V., Depaulis, A., Marescaux, C., Nehlig, A. & Le Gal La Salle, G.
838 (1999) Recurrent seizures and hippocampal sclerosis following intrahippocampal kainate
839 injection in adult mice: electroencephalography, histopathology and synaptic reorganization
840 similar to mesial temporal lobe epilepsy. *Neuroscience*, **89**, 717-729.
841
842 Bouilleret, V., Schwaller, B., Schurmans, S., Celio, M.R. & Fritschy, J.M. (2000b)
843 Neurodegenerative and morphogenic changes in a mouse model of temporal lobe epilepsy

844 do not depend on the expression of the calcium-binding proteins parvalbumin, calbindin, or
845 calretinin. *Neuroscience*, **97**, 47-58.
846
847 Buckmaster, P.S. (2012) Mossy Fiber Sprouting in the Dentate Gyrus. In Noebels, J.L.,
848 Avoli, M., Rogawski, M.A., Olsen, R.W., Delgado-Escueta, A.V. (eds) *Jasper's Basic*
849 *Mechanisms of the Epilepsies*, Bethesda (MD).
850
851 Busche, M.A., Chen, X., Henning, H.A., Reichwald, J., Staufenbiel, M., Sakmann, B. &
852 Konnerth, A. (2012) Critical role of soluble amyloid-beta for early hippocampal hyperactivity
853 in a mouse model of Alzheimer's disease. *Proc Natl Acad Sci U S A*, **109**, 8740-8745.
854
855 Chin, J., Palop, J.J., Yu, G.Q., Kojima, N., Masliah, E. & Mucke, L. (2004) Fyn kinase
856 modulates synaptotoxicity, but not aberrant sprouting, in human amyloid precursor protein
857 transgenic mice. *J Neurosci*, **24**, 4692-4697.
858
859 Colonna, M. & Wang, Y. (2016) TREM2 variants: new keys to decipher Alzheimer disease
860 pathogenesis. *Nat Rev Neurosci*, **17**, 201-207.
861
862 Deprez, F., Vogt, F., Floriou-Servou, A., Lafourcade, C., Rudolph, U., Tyagarajan, S. &
863 Fritschy, J. (2016) Partial inactivation of $GABA_A$ receptors containing the α5 subunit affects
864 the development of adult-born dentate gyrus granule cells. *Eur J Neurosci*, **44**, 2258-2271.
865
866 Diez, M., Danner, S., Frey, P., Sommer, B., Staufenbiel, M., Wiederhold, K.H. & Hokfelt, T.
867 (2003) Neuropeptide alterations in the hippocampal formation and cortex of transgenic mice
868 overexpressing beta-amyloid precursor protein (APP) with the Swedish double mutation
869 (APP23). *Neurobiol Dis*, **14**, 579-594.
870

El Bahh, B., Balosso, S., Hamilton, T., Herzog, H., Beck-Sickinger, A., Sperk, G., Gehlert, D., Vezzani, A. & Colmers, W. (2005) The anti-epileptic actions of neuropeptide Y in the hippocampus are mediated by Y2 and not Y5 receptors.
. *Eur J Neurosci*, **22**, 1417-1430.

Erickson, J.C., Clegg, K.E. & Palmiter, R.D. (1996) Sensitivity to leptin and susceptibility to seizures of mice lacking neuropeptide Y. *Nature*, **381**, 415-421.

Fisher, R.S. & Alger, B.E. (1984) Electrophysiological mechanisms of kainic acid-induced epileptiform activity in the rat hippocampal slice. *J Neurosci*, **4**, 1312-1323.

Gardoni, F., Boraso, M., Zianni, E., Corsini, E., Galli, C.L., Cattabeni, F., Marinovich, M., Di Luca, M. & Viviani, B. (2011) Distribution of interleukin-1 receptor complex at the synaptic membrane driven by interleukin-1beta and NMDA stimulation. *J Neuroinflammation*, **8**, 14.

Gotzsche, C.R., Nikitidou, L., Sorensen, A.T., Olesen, M.V., Sorensen, G., Christiansen, S.H., Angehagen, M., Woldbye, D.P. & Kokaia, M. (2012) Combined gene overexpression of neuropeptide Y and its receptor Y5 in the hippocampus suppresses seizures. *Neurobiol Dis*, **45**, 288-296.

Guo, H., Castro, P.A., Palmiter, R.D. & Baraban, S.C. (2002) Y5 receptors mediate neuropeptide Y actions at excitatory synapses in area CA3 of the mouse hippocampus. *J Neurophysiol*, **87**, 558-566.

Heneka, M.T., Kummer, M.P., Stutz, A., Delekate, A., Schwartz, S., Vieira-Saecker, A., Griep, A., Axt, D., Remus, A., Tzeng, T.C., Gelpi, E., Halle, A., Korte, M., Latz, E. & Golenbock, D.T. (2013) NLRP3 is activated in Alzheimer's disease and contributes to pathology in APP/PS1 mice. *Nature*, **493**, 674-678.

Heppner, F.L., Ransohoff, R.M. & Becher, B. (2015) Immune attack: the role of inflammation in Alzheimer disease. *Nat Rev Neurosci*, **16**, 358-372.

Hesdorffer, D.C., Hauser, W.A., Annegers, J.F., Kokmen, E. & Rocca, W.A. (1996) Dementia and adult-onset unprovoked seizures. *Neurology*, **46**, 727-730.

Horvath, A., Szucs, A., Barcs, G. & Kamondi, A. (2017) Sleep EEG Detects Epileptiform Activity in Alzheimer's Disease with High Sensitivity. *J Alzheimers Dis*, **56**, 1175-1183.

Iyengar, S.S., LaFrancois, J.J., Friedman, D., Drew, L.J., Denny, C.A., Burghardt, N.S., Wu, M.V., Hsieh, J., Hen, R. & Scharfman, H.E. (2015) Suppression of adult neurogenesis increases the acute effects of kainic acid. *Exp Neurol*, **264**, 135-149.

Jessberger, S., Romer, B., Babu, H. & Kempermann, G. (2005) Seizures induce proliferation and dispersion of doublecortin-positive hippocampal progenitor cells. *Exp Neurol*, **196**, 342-351.

Kam, K., Duffy, A.M., Moretto, J., LaFrancois, J.J. & Scharfman, H.E. (2016) Interictal spikes during sleep are an early defect in the Tg2576 mouse model of beta-amyloid neuropathology. *Sci Rep*, **6**, 20119.

Knobloch, M., Konietzko, U., Krebs, D.C. & Nitsch, R.M. (2007) Intracellular Abeta and cognitive deficits precede beta-amyloid deposition in transgenic arcAbeta mice. *Neurobiol Aging*, **28**, 1297-1306.

925 Kralic, J.E., Ledergerber, D.A. & Fritschy, J.M. (2005) Disruption of the neurogenic potential
926 of the dentate gyrus in a mouse model of temporal lobe epilepsy with focal seizures. *Eur J*
927 *Neurosci*, **22**, 1916-1927.
928
929 Lam, A.D., Deck, G., Goldman, A., Eskandar, E.N., Noebels, J. & Cole, A.J. (2017) Silent
930 hippocampal seizures and spikes identified by foramen ovale electrodes in Alzheimer's
931 disease. *Nat Med*.
932
933 Ledergerber, D., Fritschy, J.M. & Kralic, J.E. (2006) Impairment of dentate gyrus neuronal
934 progenitor cell differentiation in a mouse model of temporal lobe epilepsy. *Exp Neurol*, **199**,
935 130-142.
936
937 Mahar, I., Albuquerque, M.S., Mondragon-Rodriguez, S., Cavanagh, C., Davoli, M.A.,
938 Chabot, J.G., Williams, S., Mechawar, N., Quirion, R. & Krantic, S. (2016) Phenotypic
939 Alterations in Hippocampal NPY- and PV-Expressing Interneurons in a Presymptomatic
940 Transgenic Mouse Model of Alzheimer's Disease. *Front Aging Neurosci*, **8**, 327.
941
942 Marksteiner, J., Ortler, M., Bellmann, R. & Sperk, G. (1990) Neuropeptide Y biosynthesis is
943 markedly induced in mossy fibers during temporal lobe epilepsy of the rat. *Neurosci Lett*,
944 **112**, 143-148.
945
946 Maroso, M., Balosso, S., Ravizza, T., Liu, J., Aronica, E., Iyer, A.M., Rossetti, C., Molteni,
947 M., Casalgrandi, M., Manfredi, A.A., Bianchi, M.E. & Vezzani, A. (2010) Toll-like receptor 4
948 and high-mobility group box-1 are involved in ictogenesis and can be targeted to reduce
949 seizures. *Nat Med*, **16**, 413-419.
950
951 Marsh, D.J., Baraban, S.C., Hollopeter, G. & Palmiter, R.D. (1999) Role of the Y5
952 neuropeptide Y receptor in limbic seizures. *Proc Natl Acad Sci U S A*, **96**, 13518-13523.

953

954 Meijering, E., Jacob, M., Sarria, J.C., Steiner, P., Hirling, H. & Unser, M. (2004) Design and
955 validation of a tool for neurite tracing and analysis in fluorescence microscopy images.
956 *Cytometry A*, **58**, 167-176.

957

958 Meyer-Luehmann, M., Spires-Jones, T.L., Prada, C., Garcia-Alloza, M., de Calignon, A.,
959 Rozkalne, A., Koenigsknecht-Talboo, J., Holtzman, D.M., Bacskai, B.J. & Hyman, B.T.
960 (2008) Rapid appearance and local toxicity of amyloid-beta plaques in a mouse model of
961 Alzheimer's disease. *Nature*, **451**, 720-724.

962

963 Minkeviciene, R., Rheims, S., Dobszay, M.B., Zilberter, M., Hartikainen, J., Fulop, L., Penke,
964 B., Zilberter, Y., Harkany, T., Pitkanen, A. & Tanila, H. (2009) Amyloid beta-induced
965 neuronal hyperexcitability triggers progressive epilepsy. *J Neurosci*, **29**, 3453-3462.

966

967 Minthon, L., Edvinsson, L., Ekman, R. & Gustafson, L. (1990) Neuropeptide levels in
968 Alzheimer's disease and dementia with frontotemporal degeneration. *J Neural Transm*
969 *Suppl*, **30**, 57-67.

970

971 Notter, T., Panzanelli, P., Pfister, S., Mircsof, D. & Fritschy, J.M. (2014) A protocol for
972 concurrent high-quality immunohistochemical and biochemical analyses in adult mouse
973 central nervous system. *Eur J Neurosci*, **39**, 165-175.

974

975 Palchykova, S., Winsky-Sommerer, R., Shen, H.Y., Boison, D., Gerling, A. & Tobler, I.
976 (2010) Manipulation of adenosine kinase affects sleep regulation in mice. *J Neurosci*, **30**,
977 13157-13165.

978

979 Palop, J.J., Chin, J., Roberson, E.D., Wang, J., Thwin, M.T., Bien-Ly, N., Yoo, J., Ho, K.O.,
980 Yu, G.Q., Kreitzer, A., Finkbeiner, S., Noebels, J.L. & Mucke, L. (2007) Aberrant excitatory

neuronal activity and compensatory remodeling of inhibitory hippocampal circuits in mouse models of Alzheimer's disease. *Neuron*, **55**, 697-711.

Palop, J.J., Jones, B., Kekonius, L., Chin, J., Yu, G.Q., Raber, J., Masliah, E. & Mucke, L. (2003) Neuronal depletion of calcium-dependent proteins in the dentate gyrus is tightly linked to Alzheimer's disease-related cognitive deficits. *Proc Natl Acad Sci U S A*, **100**, 9572-9577.

Palop, J.J. & Mucke, L. (2016) Network abnormalities and interneuron dysfunction in Alzheimer disease. *Nat Rev Neurosci*, **17**, 777-792.

Parent, J.M., Yu, T.W., Leibowitz, R.T., Geschwind, D.H., Sloviter, R.S. & Lowenstein, D.H. (1997) Dentate granule cell neurogenesis is increased by seizures and contributes to aberrant network reorganization in the adult rat hippocampus. *J Neurosci*, **17**, 3727-3738.

Petrovic, M.M., Viana da Silva, S., Clement, J.P., Vyklicky, L., Mulle, C., Gonzalez-Gonzalez, I.M. & Henley, J.M. (2017) Metabotropic action of postsynaptic kainate receptors triggers hippocampal long-term potentiation. *Nat Neurosci*, **20**, 529-539.

Pinel, J.P. & Rovner, L.I. (1978) Experimental epileptogenesis: kindling-induced epilepsy in rats. *Exp Neurol*, **58**, 190-202.

Racine, R.J. (1972) Modification of seizure activity by electrical stimulation. II. Motor seizure. *Electroencephalogr Clin Neurophysiol*, **32**, 281-294.

Ramos, B., Baglietto-Vargas, D., del Rio, J.C., Moreno-Gonzalez, I., Santa-Maria, C., Jimenez, S., Caballero, C., Lopez-Tellez, J.F., Khan, Z.U., Ruano, D., Gutierrez, A. & Vitorica, J. (2006) Early neuropathology of somatostatin/NPY GABAergic cells in the

1009 hippocampus of a PS1xAPP transgenic model of Alzheimer's disease. *Neurobiol Aging*, **27**,
1010 1658-1672.
1011
1012 Riban, V., Bouilleret, V., Pham-Le, B.T., Fritschy, J.M., Marescaux, C. & Depaulis, A. (2002)
1013 Evolution of hippocampal epileptic activity during the development of hippocampal sclerosis
1014 in a mouse model of temporal lobe epilepsy. *Neuroscience*, **112**, 101-111.
1015
1016 Richichi, C., Lin, E.J., Stefanin, D., Colella, D., Ravizza, T., Grignaschi, G., Veglianese, P.,
1017 Sperk, G., During, M.J. & Vezzani, A. (2004) Anticonvulsant and antiepileptogenic effects
1018 mediated by adeno-associated virus vector neuropeptide Y expression in the rat
1019 hippocampus. *J Neurosci*, **24**, 3051-3059.
1020
1021 Roberson, E.D., Halabisky, B., Yoo, J.W., Yao, J., Chin, J., Yan, F., Wu, T., Hamto, P.,
1022 Devidze, N., Yu, G.Q., Palop, J.J., Noebels, J.L. & Mucke, L. (2011) Amyloid-beta/Fyn-
1023 induced synaptic, network, and cognitive impairments depend on tau levels in multiple
1024 mouse models of Alzheimer's disease. *J Neurosci*, **31**, 700-711.
1025
1026 Roberson, E.D., Scearce-Levie, K., Palop, J.J., Yan, F., Cheng, I.H., Wu, T., Gerstein, H.,
1027 Yu, G.Q. & Mucke, L. (2007) Reducing endogenous tau ameliorates amyloid beta-induced
1028 deficits in an Alzheimer's disease mouse model. *Science*, **316**, 750-754.
1029
1030 Sanchez, P.E., Zhu, L., Verret, L., Vossel, K.A., Orr, A.G., Cirrito, J.R., Devidze, N., Ho, K.,
1031 Yu, G.Q., Palop, J.J. & Mucke, L. (2012) Levetiracetam suppresses neuronal network
1032 dysfunction and reverses synaptic and cognitive deficits in an Alzheimer's disease model.
1033 *Proc Natl Acad Sci U S A*, **109**, E2895-2903.
1034

1035 Scarmeas, N., Honig, L.S., Choi, H., Cantero, J., Brandt, J., Blacker, D., Albert, M.,
1036 Amatniek, J.C., Marder, K., Bell, K., Hauser, W.A. & Stern, Y. (2009) Seizures in Alzheimer
1037 disease: who, when, and how common? *Arch Neurol*, **66**, 992-997.
1038
1039 Schmid, L.C., Mittag, M., Poll, S., Steffen, J., Wagner, J., Geis, H.R., Schwarz, I., Schmidt,
1040 B., Schwarz, M.K., Remy, S. & Fuhrmann, M. (2016) Dysfunction of Somatostatin-Positive
1041 Interneurons Associated with Memory Deficits in an Alzheimer's Disease Model. *Neuron*, **92**,
1042 114-125.
1043
1044 Sholl, D.A. (1953) Dendritic organization in the neurons of the visual and motor cortices of
1045 the cat. *J Anat*, **87**, 387-406.
1046
1047 Sierra, A., Martin-Suarez, S., Valcarcel-Martin, R., Pascual-Brazo, J., Aelvoet, S.A., Abiega,
1048 O., Deudero, J.J., Brewster, A.L., Bernales, I., Anderson, A.E., Baekelandt, V., Maletic-
1049 Savatic, M. & Encinas, J.M. (2015) Neuronal hyperactivity accelerates depletion of neural
1050 stem cells and impairs hippocampal neurogenesis. *Cell Stem Cell*, **16**, 488-503.
1051
1052 Song, J., Zhong, C., Bonaguidi, M.A., Sun, G.J., Hsu, D., Gu, Y., Meletis, K., Huang, Z.J.,
1053 Ge, S., Enikolopov, G., Deisseroth, K., Luscher, B., Christian, K.M., Ming, G.L. & Song, H.
1054 (2012) Neuronal circuitry mechanism regulating adult quiescent neural stem-cell fate
1055 decision. *Nature*, **489**, 150-154.
1056
1057 Sorensen, G., Wegener, G., Hasselstrom, J., Hansen, T.V., Wortwein, G., Fink-Jensen, A. &
1058 Woldbye, D.P. (2009) Neuropeptide Y infusion into the shell region of the rat nucleus
1059 accumbens increases extracellular levels of dopamine. *Neuroreport*, **20**, 1023-1026.
1060

1061 Stefanits, H., Wesseling, C. & Kovacs, G.G. (2014) Loss of Calbindin immunoreactivity in the
1062 dentate gyrus distinguishes Alzheimer's disease from other neurodegenerative dementias.
1063 *Neurosci Lett*, **566**, 137-141.
1064
1065 Sudduth, T., Greenstein, A. & Wilcock, D. (2013) Intracranial injection of Gammagard, a
1066 human IVIg, modulates the inflammatory response of the brain and lowers Aβ in APP/PS1
1067 mice along a different time course than anti-Aβ antibodies. *J Neurosci*, **33**, 9684-9692.
1068
1069 Sun, B., Halabisky, B., Zhou, Y., Palop, J.J., Yu, G., Mucke, L. & Gan, L. (2009) Imbalance
1070 between GABAergic and Glutamatergic Transmission Impairs Adult Neurogenesis in an
1071 Animal Model of Alzheimer's Disease. *Cell Stem Cell*, **5**, 624-633.
1072
1073 Suzuki, F., Junier, M.P., Guilhem, D., Sorensen, J.C. & Onteniente, B. (1995) Morphogenetic
1074 effect of kainate on adult hippocampal neurons associated with a prolonged expression of
1075 brain-derived neurotrophic factor. *Neuroscience*, **64**, 665-674.
1076
1077 Tonder, N., Kragh, J., Finsen, B.R., Bolwig, T.G. & Zimmer, J. (1994) Kindling induces
1078 transient changes in neuronal expression of somatostatin, neuropeptide Y, and calbindin in
1079 adult rat hippocampus and fascia dentata. *Epilepsia*, **35**, 1299-1308.
1080
1081 Tu, B., Timofeeva, O., Jiao, Y. & Nadler, J.V. (2005) Spontaneous release of neuropeptide Y
1082 tonically inhibits recurrent mossy fiber synaptic transmission in epileptic brain. *J Neurosci*,
1083 **25**, 1718-1729.
1084
1085 Verret, L., Jankowsky, J.L., Xu, G.M., Borchelt, D.R. & Rampon, C. (2007) Alzheimer's-type
1086 amyloidosis in transgenic mice impairs survival of newborn neurons derived from adult
1087 hippocampal neurogenesis. *J Neurosci*, **27**, 6771-6780.
1088

1089 Verret, L., Mann, E.O., Hang, G.B., Barth, A.M., Cobos, I., Ho, K., Devidze, N., Masliah, E.,
1090 Kreitzer, A.C., Mody, I., Mucke, L. & Palop, J.J. (2012) Inhibitory interneuron deficit links
1091 altered network activity and cognitive dysfunction in Alzheimer model. *Cell*, **149**, 708-721.
1092
1093 Vezzani, A., Ravizza, T., Moneta, D., Conti, M., Borroni, A., Rizzi, M., Samanin, R. & Maj, R.
1094 (1999) Brain-derived neurotrophic factor immunoreactivity in the limbic system of rats after
1095 acute seizures and during spontaneous convulsions: temporal evolution of changes as
1096 compared to neuropeptide Y. *Neuroscience*, **90**, 1445-1461.
1097
1098 Vezzani, A. & Viviani, B. (2015) Neuromodulatory properties of inflammatory cytokines and
1099 their impact on neuronal excitability. *Neuropharmacology*, **96**, 70-82.
1100
1101 Viviani, B., Bartesaghi, S., Gardoni, F., Vezzani, A., Behrens, M.M., Bartfai, T., Binaglia, M.,
1102 Corsini, E., Di Luca, M., Galli, C.L. & Marinovich, M. (2003) Interleukin-1beta enhances
1103 NMDA receptor-mediated intracellular calcium increase through activation of the Src family
1104 of kinases. *J Neurosci*, **23**, 8692-8700.
1105
1106 Vossel, K.A., Beagle, A.J., Rabinovici, G.D., Shu, H., Lee, S.E., Naasan, G., Hegde, M.,
1107 Cornes, S.B., Henry, M.L., Nelson, A.B., Seeley, W.W., Geschwind, M.D., Gorno-Tempini,
1108 M.L., Shih, T., Kirsch, H.E., Garcia, P.A., Miller, B.L. & Mucke, L. (2013) Seizures and
1109 epileptiform activity in the early stages of Alzheimer disease. *JAMA Neurol*, **70**, 1158-1166.
1110
1111 Vossel, K.A., Ranasinghe, K.G., Beagle, A.J., Mizuiri, D., Honma, S.M., Dowling, A.F.,
1112 Darwish, S.M., Van Berlo, V., Barnes, D.E., Mantle, M., Karydas, A.M., Coppola, G.,
1113 Roberson, E.D., Miller, B.L., Garcia, P.A., Kirsch, H.E., Mucke, L. & Nagarajan, S.S. (2016)
1114 Incidence and impact of subclinical epileptiform activity in Alzheimer's disease. *Ann Neurol*,
1115 **80**, 858-870.
1116

1117 Wang, Y., Cella, M., Mallinson, K., Ulrich, J.D., Young, K.L., Robinette, M.L., Gilfillan, S.,
1118 Krishnan, G.M., Sudhakar, S., Zinselmeyer, B.H., Holtzman, D.M., Cirrito, J.R. & Colonna,
1119 M. (2015) TREM2 lipid sensing sustains the microglial response in an Alzheimer's disease
1120 model. *Cell*, **160**, 1061-1071.
1121
1122 Westmark, C.J., Westmark, P.R., Beard, A.M., Hildebrandt, S.M. & Malter, J.S. (2008)
1123 Seizure susceptibility and mortality in mice that over-express amyloid precursor protein. *Int J*
1124 *Clin Exp Pathol*, **1**, 157-168.
1125
1126 Woldbye, D.P., Angehagen, M., Gotzsche, C.R., Elbrond-Bek, H., Sorensen, A.T.,
1127 Christiansen, S.H., Olesen, M.V., Nikitidou, L., Hansen, T.V., Kanter-Schlifke, I. & Kokaia, M.
1128 (2010) Adeno-associated viral vector-induced overexpression of neuropeptide Y Y2
1129 receptors in the hippocampus suppresses seizures. *Brain*, **133**, 2778-2788.
1130
1131 Woldbye, D.P., Larsen, P.J., Mikkelsen, J.D., Klemp, K., Madsen, T.M. & Bolwig, T.G. (1997)
1132 Powerful inhibition of kainic acid seizures by neuropeptide Y via Y5-like receptors. *Nat Med*,
1133 **3**, 761-764.
1134
1135 Woldbye, D.P., Madsen, T.M., Larsen, P.J., Mikkelsen, J.D. & Bolwig, T.G. (1996)
1136 Neuropeptide Y inhibits hippocampal seizures and wet dog shakes. *Brain Res*, **737**, 162-
1137 168.
1138
1139 Zattoni, M., Mura, M.L., Deprez, F., Schwendener, R.A., Engelhardt, B., Frei, K. & Fritschy,
1140 J.M. (2011) Brain infiltration of leukocytes contributes to the pathophysiology of temporal
1141 lobe epilepsy. *J Neurosci*, **31**, 4037-4050.
1142
1143
1144

Figure legends

Figure 1

Area selection in histological sections for quantitative analysis. A, For densitometry analysis, square boxes were placed in different layers of the dorsal hippocampus. B, For stereological analysis, the molecular (ML) and the granule cell layer (GCL) of the dentate gyrus were outlined. CA1, cornu ammonis subfield 1; SO, stratum oriens; SP, stratum pyramidale; SR, stratum radiatum; SLM, stratum lacunosum moleculare; HL, hilus.

Figure 2

Increased response of ArcticAβ mice to IHK-induced epilepsy. A, Schematic representation of the experimental design to assess acquired epilepsy. Kainic acid injection and electrode implantation were performed in the right dorsal hippocampus, while EEGs were recorded and tissue was collected for histological analysis at 21 dpi. B, Cresyl violet staining of the ipsilateral hippocampus. Neurodegeneration in CA1, CA3c, and the hilus, along with the dispersion of dentate granule cells, show a similar pattern in both IHK-injected (SO, stratum oriens; SP, stratum pyramidale; SR, stratum radiatum; SLM, stratum lacunosum moleculare; ML, molecular layer; GCL, granule cell layer; HL, hilus). C, F4/80+ macrophages invading the ipsilateral dentate gyrus and the dispersion of dentate granule cells. Stereological quantification of F4/80+ macrophages and measuring the layer thickness of GCL and ML revealed no differences between genotypes (n = 6/genotype; 3-4 sections; unpaired t-tests). D, Densitometric analysis of CD68 staining. Microglial activation was increased 3 weeks after IHK injection in the ipsilateral hemisphere of both genotypes (n = 6/genotype; 3-4 sections; ***$P < 0.0001$, two-way ANOVA). E, Frequency of spontaneous recurrent seizures (SRS). Both genotypes show a similar number of seizures three weeks after IHK. Representative traces of intrahippocampal recordings reveal a high frequency of SRS in the IHK model of acquired epilepsy (box outlines 10 s and 15 mV). F, Survival curve during

epileptogenesis. ArcticAβ mice (n = 20) exhibit an increased mortality rate during the status epilepticus and during the transition from the latent to the chronic period with SRS in comparison to their wildtype littermates (n = 8) (***P = 0.0003, Mantel-Cox test). Quantitative data represent mean ± SEM. Scale bars, 150 µm.

Figure 3

Decreased synaptic strength and increased KA-induced LTP in slices of ArcticAβ mice. A, Schematic diagram showing electrode placement (Stim = bipolar stimulation electrode, Rec = recording electrode) and hippocampal regions (S. coll = Schaffer collateral, DG = dentate gyrus, CA1 and 3 = areas Cornu Ammonis 1 and 3 respectively). B, Current - voltage relationship. ArcticAβ mice show a decreased synaptic strength compared to wildtype littermates (**P < 0.01). Linear regression lines used for statistical comparison are dashed. C, KA-induced LTP is more pronounced in ArcticAβ mice. Upper inset: representative traces of population spikes before (black traces) and 30 min after (blue trace) a 10-min application of 1 µM KA. Paired pulses were given 50 ms apart. Stimulation artifacts were removed for visual clarity. D, Percent change per cell before and 30 min after a 10-min application of 1 µM KA. The increase in PS amplitude is significant for both groups after application of 1µM KA (P = 0.02, two-way repeated measure ANOVA), and between wildtype and ArcticAβ mice in the degree of potentiation after a 30-min washout period (P = 0.01, two-way repeated measure ANOVA). E, Paired-pulse ratio before and 30 min after a 10-min application of 1 µM KA. Quantitative data represent mean ± SEM.

Figure 4

Reduced frequency of spontaneous inhibitory currents after KA application in slices of ArcticAβ mice. A, Schematic diagram of a hippocampal slice after removal of the CA3 area. B, Top inset: representative traces. Bottom graphs: Cumulative frequency distribution plots

illustrating the frequency and amplitude of sIPSCs. Frequency of events is similar in wildtype and ArcticAβ mice, but a 5-min application of KA decreases the inter-event interval in ArcticAβ mice significantly ($P < 0.0001$, Kolmogorov–Smirnoff test). The sIPSC amplitude is higher in ArcticAβ mice under baseline conditions ($P < 0.0001$, Kolmogorov–Smirnoff test), but not after KA application. C, Distribution of clustered activity, consisting of events that are separated by <100 ms. KA uncovers clusters with a higher number of events in wildtype mice, whereas the opposite is found in ArcticAβ mice. (n = 4-5 mice/genotype).

Figure 5

Severe status epilepticus and early onset of SRS in ArcticAβ mice. A, Schematic representation of the experimental design to monitor EEG activity during early epileptogenesis. Continuous vEEG recordings were performed for 18 days after IHK injection. B, Percentage of convulsive seizures with severity 2-8 according to the Racine-Pinel-Rovner scale during status epilepticus (Table 1). While ArcticAβ mice had more severe seizures than wildtype mice after IHK injection (left), both genotypes had seizures with severity 2-3 when treated with diazepam immediately after IHK injection (right). C, Total number of convulsive (left) and non-convulsive (right) seizures during status epilepticus. Diazepam significantly reduced the number of seizures (n = 4-6 mice/genotype; $*P < 0.05$, $****P < 0.0001$, two-way ANOVA). D, Duration of convulsive behavioral seizures of severity 2-8. There was no difference between genotypes (unpaired t-test). E, Characterization of EEG patterns during the latent phase and beginning of chronic phase. An early onset of short SRS-like events (defined as seizures with a duration of 10-20 s) occurred in ArcticAβ mice at 5-8 dpi, while regular SRS were detected already at 3 dpi in the two mice that died later on. Bottom traces depict representative examples of an SRS-like event ($10 \text{ s} < \Delta t < 20 \text{ s}$), a regular SRS ($\geq 20$ s), and a tonic-clonic seizure leading to the death of the animal. The spectrogram in the bottom left corner depicts the increase power in the frequency

range of 20-100 Hz that is characteristic for seizures. F, Mortality rate for mice receiving diazepam after IHK injection. With diazepam, status epilepticus-associated mortality in ArcticAβ mice is abrogated, but some transgenic mice still died during the transition from the latent to the chronic phase. Quantitative data represent mean ± SEM.

Figure 6

Reduced microgliosis in ArcticAβ mice during epileptogenesis. A, Representative images of a marker for microglial activation (CD68) at 3, 6 and 14 dpi compared to control levels. Scale bar, 250 μm. B, Densitometric analysis of CD68-IR in controls, in mice dying during SE, as well as at 1, 3, 6, and 14 dpi. Both ArcticAβ mice (n = 4-5/ time point; red stars) and wildtype littermates (n = 5-7/ time point; black stars) showed increased CD68-IR compared to baseline control over the time course of early epileptogenesis in all layers of the ipsilateral and in some layers of the contralateral hippocampus (*P < 0.05, **P < 0.01, ***P < 0.001, ****P < 0.0001; two-way ANOVA, Bonferroni post-hoc test). Analysis revealed a significant group difference in the SO of CA3a,b and the hilus (green stars; compare Table 5 for details). Data represent mean ± SEM normalized to control for each region.

Figure 7

Impaired epileptogenesis-associated increase of neuropeptide Y in ArcticAβ mice. A, Representative images of NPY staining of both genotypes comparing controls to mice 24 h after IHK injection, the peak of the NPY upregulation. NPY-IR increases bilaterally particularly in mossy fibers in the hilus and CA3. Scale bar, 250 μm. B, Densitometric analysis of NPY-IR. IHK-injected mice show a significant increase in NPY levels in the ML, GCL, HL and CA3c (black and red stars denote significant increase compared to control in wildtype and in mutant mice, respectively. A comparison between genotypes (green stars) reveals a significantly higher NPY-IR in the contralateral ML, HL, and CA3c as well as

ipsilateral hilus of wildtype mice compared to ArcticAβ mice at 1 and 3 dpi (*P < 0.05, **P < 0.01, ***P < 0.001, ****P < 0.0001; two-way ANOVA, Bonferroni post-hoc test). Quantitative data represent mean ± SEM.

Figure 8

Reduced neuropeptide Y expression is an early, pre-plaque sequelae of AD pathology. A-D, Hippocampal expression of genes related to NPY signaling. The expression of NPY is reduced in both 3- and 9-month-old ArcticAβ mice. Regarding NPY receptors, Npy1r expression does not change, while the expression of Npy2r is increased at nine months and Npy5r decreased at three months in ArcticAβ mice. (n = 4-7; *P < 0.05, **P < 0.01; two-way ANOVA, Bonferroni post-hoc test). Quantitative data represent mean ± SEM. E, Representative images of NPY-IR from 3-and 9-month-old wildtype and ArcticAβ mice. Both genotypes reveal a similar NPY-IR at both time points. However, at nine months, three of seven ArcticAβ mice reveal weak ectopic NPY-IR in mossy fibers visible in the hilus and CA3a,b (arrowhead). F, Representative images of ZnT3-IR in 3-month-old wildtype and ArcticAβ mice. There is no obvious axonal sprouting in the molecular layer in either genotype (dashed box). G, Representative images of CB-IR in ArcticAβ mice and wildtype littermates at three months. CB-IR in mossy fibers of CA3 (solid box) and in the granule cell layer of the dentate gyrus (dashed box) are comparable between genotypes. Scale bars, 250 μm.

Figure 9

AD pathology and neuroinflammation. A, Representative images of tissue section stained for β-amyloid (6E10-IR) from 15-month-old ArcticAβ and wildtype mice. Only transgenic mice show plaques with their characteristic dense core morphology. The framed areas are enlarged below. B, Representative images of CD68-IR in hippocampal sections from 3- and

9-month-old ArcticAβ and wildtype mice. From their appearance in ArcticAβ mice at nine months of age, plaques are surrounded by activated microglia, strongly positive for CD68 and for 6E10; framed areas are enlarged below. C, Densitometric analysis of CD68-IR revealed no difference between genotypes at both the pre-plaque (three months) and the early-plaque (nine months) stage (n = 6/group; one-way ANOVA). C-E, Hippocampal expression of cytokines IL10, IL1β, and TNF. While the expression of IL10 decreased over time ($F_{(1,16)}$ = 10.96, P = 0.0044) and IL1β differed between genotypes ($F_{(1,16)}$ = 4.655, P = 0.0465), TNF expression did not change. F, The expression of Trem2, a marker for microglial phagocytosis of β-amyloid peptides and apoptotic neurons without inflammation. ArcticAβ mice show a significant increase in Trem2 expression at nine months of age, when β-amyloid plaques start to appear. Scale bars, 250 μm.

Figure 10

Increased proliferation of newborn cells and reduced spine density in ArcticAβ mice. A, Schematic representation of the experimental design to quantify newborn neurons. Mice received BrdU injections for two consecutive days and brain tissue was collected at day 1 and 28 post-BrdU injection to evaluate cell proliferation and survival rate, respectively. B, Quantification and representative images of BrdU immunostaining 1 and 28 days after the last BrdU treatment. BrdU+ cells were located in the inner part of the GCL. Higher density of BrdU+ cells was common in ArcticAβ mice at 1 dpi, but there were no differences at 28 dpi (*P > 0.05, unpaired t-test). Scale bar, 160 μm. C, Schematic representation of the experimental design to assess the dendritic arborization and spine density in adult-born neurons. Brain tissue of both genotypes was collected 21 and 42 days after the intrahippocampal injection of eGFP retrovirus. Quantification of dendritic arborization was done by Sholl analysis measuring the number of intersections between eGFP+ dendrites and virtual concentric circles centered on the cell body and spaced by 10 μm (bottom). D,

Fluorescent images of representative examples of eGFP+ cells in each genotype at 21 and 42 dpi. Quantitative result of Sholl analysis showed no significant difference, but a trend towards a reduced dendritic arborization in ArcticAβ compared to wildtype mice at 21 dpi. There were no differences between genotypes at 42 dpi. Scale bar, 50 μm. E, Dendritic spine classification analysis. Representative images of dendritic segments from eGFP expressing GCs of wildtype and ArcticAβ mice at 21 and 42 dpi (scale bar, 5μm). Quantification of mushroom, stubby, thin and overall spine density. ArcticAβ mice had significantly reduced overall spine density and specifically thin spine density at 21 dpi and a reduced stubby spine density at 42 dpi with no difference in the overall spine density (*P > 0.05, unpaired t-test). There were no genotype differences for the proportion of the three types of spines. Quantitative data represent mean ± SEM.

Figure 11

Gradual decrease of DCX+ progenitor cells in the ipsilateral SGZ during epileptogenesis. A, Representative images of the neurogenic niche in the dentate gyrus of wildtype and ArcticAβ mice. Over the course of epileptogenesis, DCX-IR in the SGZ of the ipsilateral dentate gyrus gradually decreases in both genotypes up to almost complete disappearance at 14 dpi while it remains unchanged on the contralateral side; A1, densitometric analysis of DCX-IR confirming this result (***P < 0.001, ****P < 0.0001; two-way ANOVA). Scale bar, 200 μm. B, Illustration and quantification of ectopic cells in the hilus. B, Ectopic cells were detected by triple staining for DCX (neuronal marker), GFAP (astrocytic marker) and CD68 (microglial marker). Left panel illustrates DCX-positive cells in the hilus (arrowheads), which are not stained for GFAP and CD68 (right panel); examples glial cells are indicated by arrows. B1, Quantification: the number of ectopic DCX-positive cells in the hilus was similar between ArcticAβ mice and wildtype littermates (two-way ANOVA). Quantitative data represent mean ± SEM.

Figure 12

Clearance of soluble Aβ species ameliorates epileptic phenotype in 3-month-old ArcticAβ mice during early epileptogenesis. A, Schematic representation of the experimental design using the anti-Aβ antibody, 6E10. Three days before the unilateral IHK injection, ArcticAβ mice were intracerebroventricularly (icv) injected with either 6E10 or control IgG into both hemispheres near the dorsal hippocampus. After injecting IHK, mice were monitored by vEEG to assess early onset of seizures in ArcticAβ mice. B, Characterization of EEG pattern during the latent period. IgG-treated ArcticAβ mice exhibited multiple SRS-like events and regular SRS, whereas mice injected with 6E10 showed only a few SRS-like events and short single or grouped spikes. B1, Example of IgG-injected mouse that had few SRS-like events within the analysis window; this animal had a high number of spikes clusters that were sometimes followed by a SRS-like event occurring outside of the window chosen for analysis. B2, This 6E10-injected mouse showed almost exclusively single or grouped spikes with typical frequency and power characteristics (spectrogram below). Scale bars, 500 μV, 5 s. C, Cresyl violet staining of the ipsilateral hippocampus. C, Both IgG (C1) and 6E10 (C2) pre-treated animals showed the characteristic neurodegenerative pattern seen after IHK injection, including degeneration of pyramidal cells in CA1 (black arrowheads), CA3c (red arrowhead), and the cells in the hilus (yellow arrowheads). The mouse illustrated in (B2) shared these typical histopathological hallmarks (C3). Note the absence of GC dispersion in both groups. Scale bars, 150 μm.

Table 1 Modified Racine Scale for Behavioral Seizures

Scale	Stage	Behavior
Racine behavioral scale	1	Oro-alimentary movements
	2	Head nodding
	3	Anterior limb clonus
	4	Dorsal extension (rearing)
	5	Loss of balance and falling
Pinel and Rovner behavioral scale	6	Repeated falling
	7	Strong jumping and running
	8	Stage 7 with tonic period

The table was adapted from (Pinel & Rovner, 1978).

Table 2 List of primers for RT-qPCR

Target	Forward sequence 5' → 3'	Reverse sequence 5' → 3'
Npy1r	CAAGATATACATTCGCTTGA	AGATTGTGGTTGCAGG
Npy2r	CCATCTTCCGGGAATAC	TGACGTGGTTCCTCAG
Npy5r	TCAAGCGTTCCCTCAC	ACAACAGGACATCATGC
NPY	TGGACTGACCCTCGCTCTAT	TGTCTCAGGGCTGGATCTCT
IL10	GGGAAGAGAAACCAGGGAGAT	GCCACAGTTTTCAGGGATGA
TREM2	GACCTCTCCACCAGTTTCTCC	TACATGACACCCTCAAGGACTG
TNFa	AGCCAGGAGGGAGAACAGA	CAGTGAGTGAAAGGGACAGAAC
IL1β	CAACCAACAAGTGATATTCTCCAT	GGGTGTGCCGTCTTTCATTA
Eef1a1	AAGCCCATGTGTGTTGAGAG	CTCCAGCAGCCTTCTTGTC
HPRT1	TCCTCCTCAGACCGCTTTT	AGGTATACAAAACAAATCTAGGTCAT

Table 3 List of primary antibodies for immunohistochemistry

TARGET	HOST SPECIES	DILUTION	CAT. NO.	COMPANY / ORIGIN
BrdU	**RAT**	1:1000	OBT0030	Oxford Biotech
CD68	**RAT**	1:2000	MCA1957GA	AbD Serotec
DCX	**GUINEA PIG**	1:2000	AB2253	Merck Millipore
F4/80	**RAT**	1:1000	b6640	Abcam
GFAP	**RABBIT**	1:20'000	Z334	Dako
NPY	**RABBIT**	1:1000	T-4069	Peninsula Lab.
ZnT3	**RABBIT**	1:1000	197002	Synaptic Systems

Table 4 Statistical analysis of CD68-immunoreactivity after intra-hippocampal KA injection

Area	Source of variance	F value	P value
CA1 - SO	Inter	F (9, 80) = 1.486	P=0.1674
	Geno	F (1, 80) = 3.723	P=0.0572
	Time	F (9, 80) = 28.97	P<0.0001
CA1 - SP	Inter	F (9, 80) = 1.282	P=0.2598
	Geno	F (1, 80) = 3.237	P=0.0758
	Time	F (9, 80) = 56.68	P<0.0001
CA1 - SR	Inter	F (9, 80) = 1.338	P=0.2309
	Geno	**F (1, 80) = 4.28**	**P=0.0418**
	Time	F (9, 80) = 16.5	P<0.0001
SLM	Inter	F (9, 80) = 0.7	P=0.7070
	Geno	F (1, 80) = 1.492	P=0.2256
	Time	F (9, 80) = 25.7	P<0.0001
ML	Inter	F (9, 80) = 0.7915	P=0.6249
	Geno	F (1, 80) = 0.06475	P=0.7998
	Time	F (9, 80) = 12.13	P<0.0001
GCL	Inter	F (9, 79) = 1.006	P=0.4425
	Geno	F (1, 79) = 1.653	P=0.2023
	Time	F (9, 79) = 8.004	P<0.0001
HL	Inter	F (9, 79) = 1.738	P=0.0940
	Geno	**F (1, 79) = 4.389**	**P=0.0394**
	Time	F (9, 79) = 17.29	P<0.0001
CA3c	Inter	F (9, 80) = 0.4201	P=0.9208
	Geno	F (1, 80) = 2.593	P=0.1112
	Time	F (9, 80) = 36.45	P<0.0001
CA3a,b - SO	Inter	F (9, 77) = 2.006	P=0.0498
	Geno	F (1, 77) = 1.286	P=0.2602
	Time	F (9, 77) = 11.22	P<0.0001
CA3a,b - SP	Inter	F (9, 77) = 0.7629	P=0.6506
	Geno	F (1, 77) = 0.6179	P=0.4342
	Time	F (9, 77) = 11.91	P<0.0001
CA3a,b - SR	Inter	F (9, 77) = 0.9621	P=0.4777
	Geno	**F (1, 77) = 8.415**	**P=0.0048**
	Time	F (9, 77) = 11.61	P<0.0001
Lucidum	Inter	F (9, 77) = 1.263	P=0.2707
	Geno	F (1, 77) = 0.3842	P=0.5372
	Time	F (9, 77) = 16.16	P<0.0001

Densitometric analysis of CD68-IR was performed ispilaterally in the regions indicated at four time-points post-IHK (1, 3, 6, and 14 dpi) as well as in controls. (see Fig. 6). Statistically significant differences among genotypes are indicated in bold. SO, stratum oriens; SP,

1353 stratum pyramidale; SR, stratum radiatum; SLM, stratum lacunosum moleculare; ML,
1354 molecular layer; GCL, granule cell layer; HL, hilus.
1355

1356 **Table 5 Statistical analysis of NPY-immunoreactivity**

Area	Source of Variance	F value	P value
ML	Inter	F (9, 78) = 3.062	P=0.0034
	Geno	**F (1, 78) = 13.97**	**P=0.0004**
	Time	F (9, 78) = 8.029	P<0.0001
GCL	Inter	F (9, 78) = 1.757	P=0.0901
	Geno	**F (1, 78) = 13.6**	**P=0.0004**
	Time	F (9, 78) = 15.85	P<0.0001
HL	Inter	F (9, 78) = 4.85	P<0.0001
	Geno	**F (1, 78) = 67.47**	**P<0.0001**
	Time	F (9, 78) = 15.52	P<0.0001
CA3c	Inter	F (9, 78) = 2.584	P=0.0116
	Geno	**F (1, 78) = 44.9**	**P<0.0001**
	Time	F (9, 78) = 12.48	P<0.0001
CA3a,b - SO	Inter	F (9, 77) = 0.6358	P=0.7631
	Geno	F (1, 77) = 2.937	P=0.0906
	Time	F (9, 77) = 1.16	P=0.3322
CA3a,b - SP	Inter	F (9, 77) = 0.7915	P=0.6250
	Geno	F (1, 77) = 0.1921	P=0.6624
	Time	F (9, 77) = 1.48	P=0.1703
CA3a,b - SR	Inter	F (9, 77) = 0.4054	P=0.9286
	Geno	F (1, 77) = 3.654	P=0.0597
	Time	F (9, 77) = 0.8237	P=0.5963
Lucidum	Inter	F (9, 77) = 0.5332	P=0.8461
	Geno	F (1, 77) = 2.248	P=0.1379
	Time	F (9, 77) = 3.357	P=0.0016

1357 Densitometric analysis of NPY-IR in ArticAβ mice and wildtype littermates was performed
1358 in the regions indicated at five time-points post-IHK (see Fig. 7). Statistically significant
1359 differences among genotypes are indicated in bold. SO, stratum oriens; SP, stratum
1360 pyramidale; SR, stratum radiatum; SLM, stratum lacunosum moleculare; ML, molecular
1361 layer; GCL, granule cell layer; HL, hilus.

1362

Table 6 Statistical analysis of CD-68 immunoreactivity in young and aged mice

Area	Source of variance	F value	P value
CA1 - SO	Inter	F (1, 20) = 2.40	P=0.1369
	Geno	F (1, 20) = 2.34	P=0.1417
	Age	F (1, 20) = 3.08	P=0.0943
CA1 - SP	Inter	F (1, 20) = 2.55	P=0.1259
	Geno	F (1, 20) = 2.07	P=0.1652
	Age	F (1, 20) = 18.05	P=0.0004
CA1 - SR	Inter	F (1, 20) = 1.60	P=0.2206
	Geno	F (1, 20) = 1.26	P=0.2756
	Age	F (1, 20) = 1.51	P=0.2334
SLM	Inter	F (1, 20) = 0.60	P=0.4485
	Geno	F (1, 20) = 1.61	P=0.2195
	Age	F (1, 20) = 14.00	P=0.0013
ML	Inter	F (1, 20) = 1.49	P=0.2362
	Geno	F (1, 20) = 2.68	P=0.1174
	Age	F (1, 20) = 2.84	P=0.1073
GCL	Inter	F (1, 20) = 2.61	P=0.1217
	Geno	F (1, 20) = 3.69	P=0.0692
	Age	F (1, 20) = 11.83	P=0.0026
HL	Inter	F (1, 20) = 0.09	P=0.7701
	Geno	F (1, 20) = 0.68	P=0.4192
	Age	F (1, 20) = 0.77	P=0.3921
CA3c	Inter	F (1, 20) = 1.03	P=0.3229
	Geno	F (1, 20) = 2.98	P=0.0995
	Age	F (1, 20) = 2.89	P=0.1044
CA3a,b	Inter	F (1, 20) = 1.41	P=0.2483
	Geno	F (1, 20) = 3.77	P=0.0664
	Age	F (1, 20) = 49.70	P<0.0001

Densitometric analysis of CD68-IR in hippocampal sections from 3- and 9-month-old ArcticAβ and wildtype mice (see Fig. 9B). No significant difference was observed in any of the regions analysed (2-way ANOVA). SO, stratum oriens; SP, stratum pyramidale; SR, stratum radiatum; SLM, stratum lacunosum moleculare; ML, molecular layer; GCL, granule cell layer; HL, hilus.

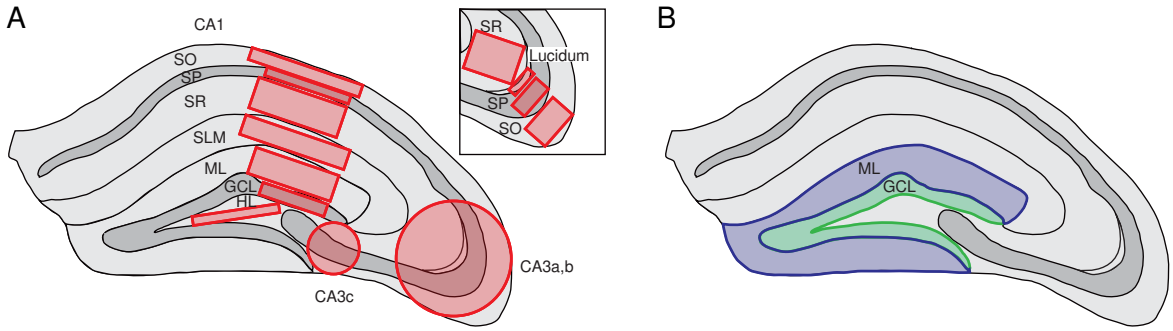

Figure 1

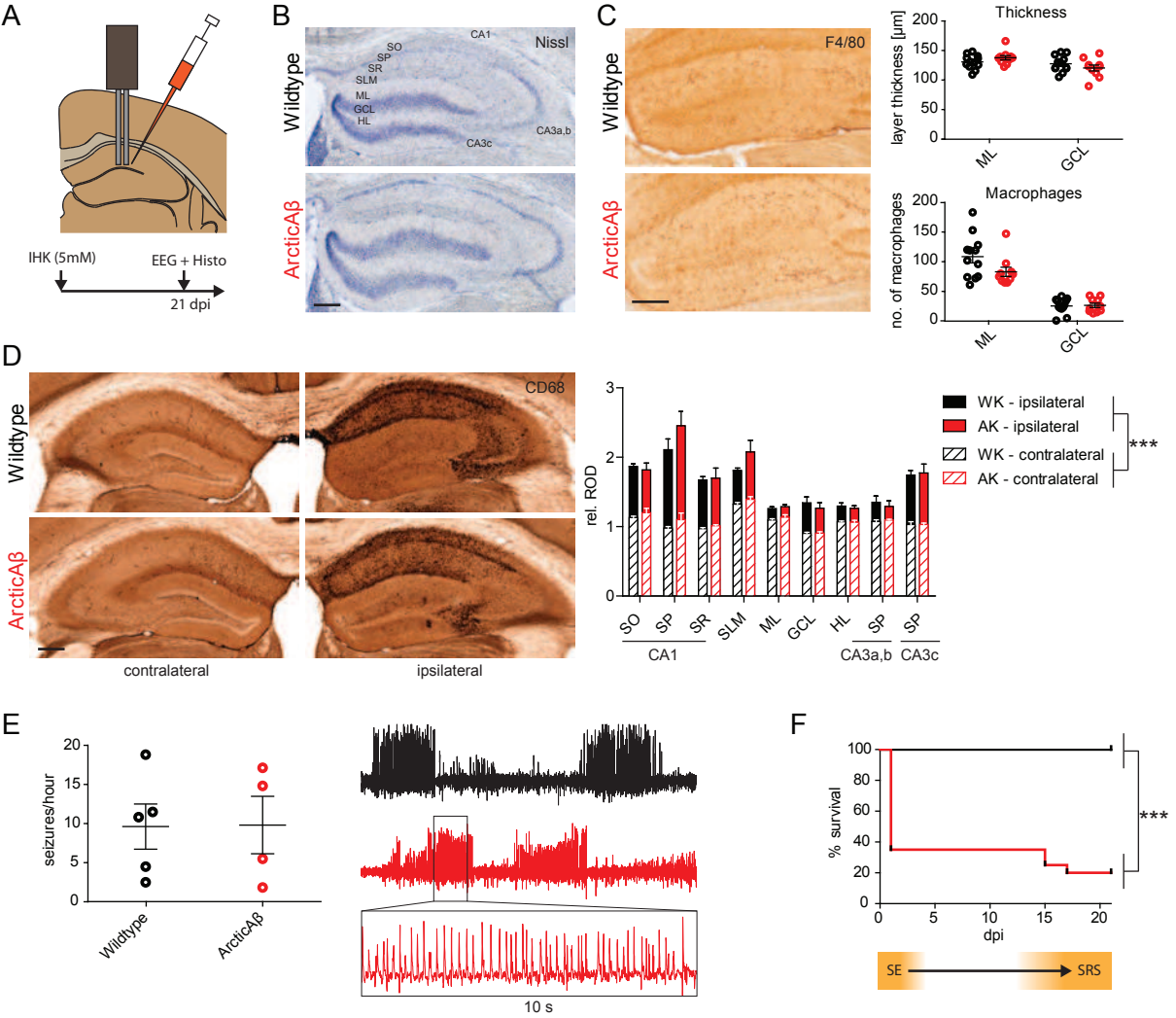
A
IHK (5mM)
EEG + Histo
21 dpi
B
Wildtype
ArcticAβ
Nissl
CA1
SO
SP
SR
SLM
ML
GCL
HL
CA3c
CA3a,b
C
Wildtype
ArcticAβ
F4/80
Thickness
layer thickness [µm]
200
150
100
50
0
ML
GCL
Macrophages
no. of macrophages
200
150
100
50
0
ML
GCL
D
Wildtype
ArcticAβ
CD68
contralateral
ipsilateral
rel. ROD
3
2
1
0
WK - ipsilateral
AK - ipsilateral
WK - contralateral
AK - contralateral
***
SO
SP
SR
SLM
ML
GCL
HL
SP
SP
CA1
CA3a,b
CA3c
E
seizures/hour
20
15
10
5
0
Wildtype
ArcticAβ
10 s
F
% survival
100
80
60
40
20
0
0
5
10
15
20
dpi
***
SE
SRS

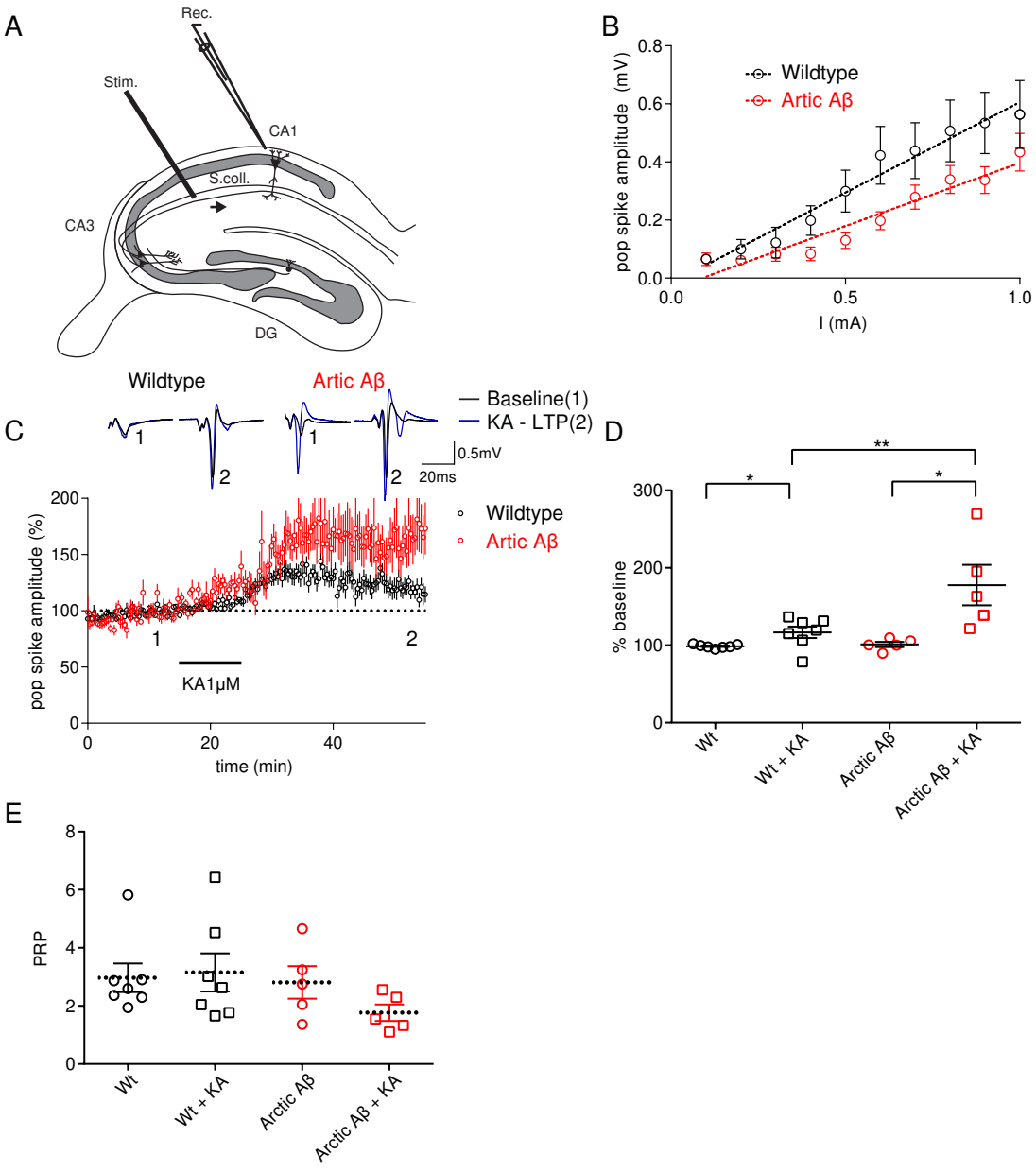
A
Rec.
Stim.
CA1
S.coll.
CA3
DG
B
Wildtype
Artic Aβ
pop spike amplitude (mV)
I (mA)
C
Wildtype
Artic Aβ
Baseline(1)
KA - LTP(2)
0.5mV
20ms
pop spike amplitude (%)
KA1μM
time (min)
D
% baseline
Wt
Wt + KA
Arctic Aβ
Arctic Aβ + KA
E
PRP
Wt
Wt + KA
Arctic Aβ
Arctic Aβ + KA

Figure 3

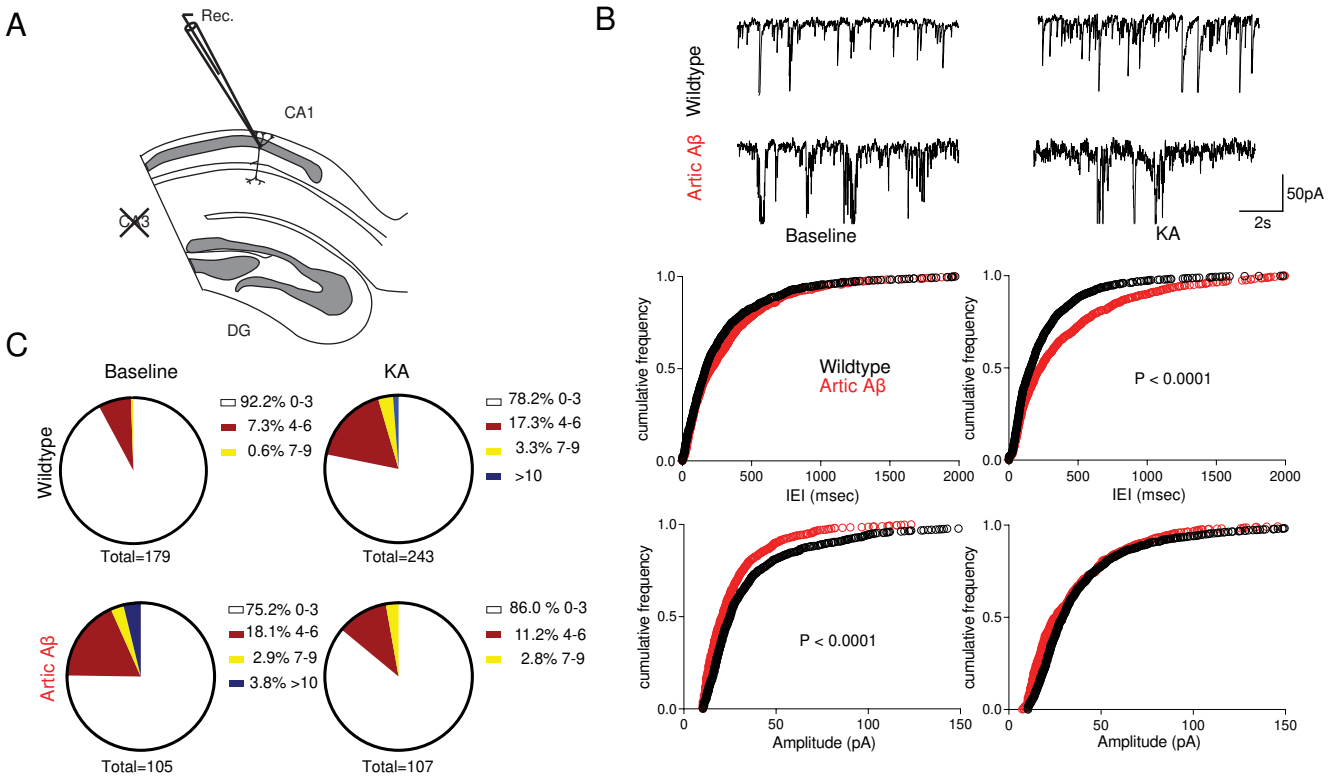
A
Rec.
CA1
CA3
DG
B
Wildtype
Artic Aβ
Baseline
KA
50pA
2s
cumulative frequency
Wildtype
Artic Aβ
P < 0.0001
IEI (msec)
Amplitude (pA)
C
Baseline
KA
Wildtype
Artic Aβ
92.2% 0-3
7.3% 4-6
0.6% 7-9
78.2% 0-3
17.3% 4-6
3.3% 7-9
>10
Total=179
Total=243
75.2% 0-3
18.1% 4-6
2.9% 7-9
3.8% >10
86.0 % 0-3
11.2% 4-6
2.8% 7-9
Total=105
Total=107

Figure 4

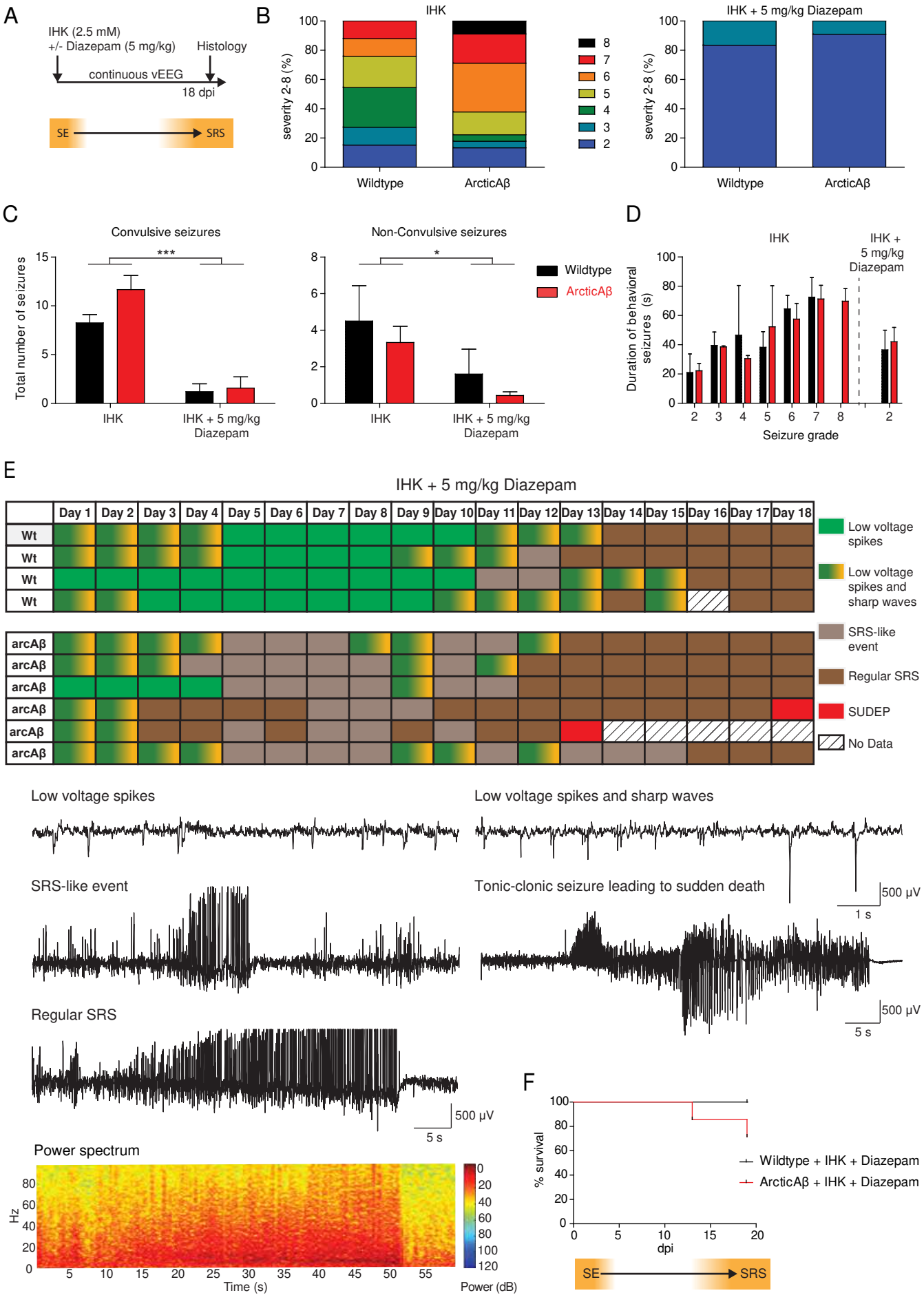
A
IHK (2.5 mM)
+/- Diazepam (5 mg/kg)
Histology
continuous vEEG
18 dpi
SE
SRS
B
IHK
severity 2-8 (%)
Wildtype
ArcticAβ
8
7
6
5
4
3
2
IHK + 5 mg/kg Diazepam
C
Convulsive seizures
Total number of seizures
***
IHK
IHK + 5 mg/kg Diazepam
Non-Convulsive seizures
*
Wildtype
ArcticAβ
D
IHK
IHK + 5 mg/kg Diazepam
Duration of behavioral seizures (s)
Seizure grade
E
IHK + 5 mg/kg Diazepam
Day 1
Day 2
Day 3
Day 4
Day 5
Day 6
Day 7
Day 8
Day 9
Day 10
Day 11
Day 12
Day 13
Day 14
Day 15
Day 16
Day 17
Day 18
Wt
arcAβ
Low voltage spikes
Low voltage spikes and sharp waves
SRS-like event
Regular SRS
SUDEP
No Data
Low voltage spikes
Low voltage spikes and sharp waves
SRS-like event
Tonic-clonic seizure leading to sudden death
500 µV
1 s
Regular SRS
500 µV
5 s
Power spectrum
Hz
Time (s)
Power (dB)
F
% survival
dpi
Wildtype + IHK + Diazepam
ArcticAβ + IHK + Diazepam
SE
SRS

Figure 5

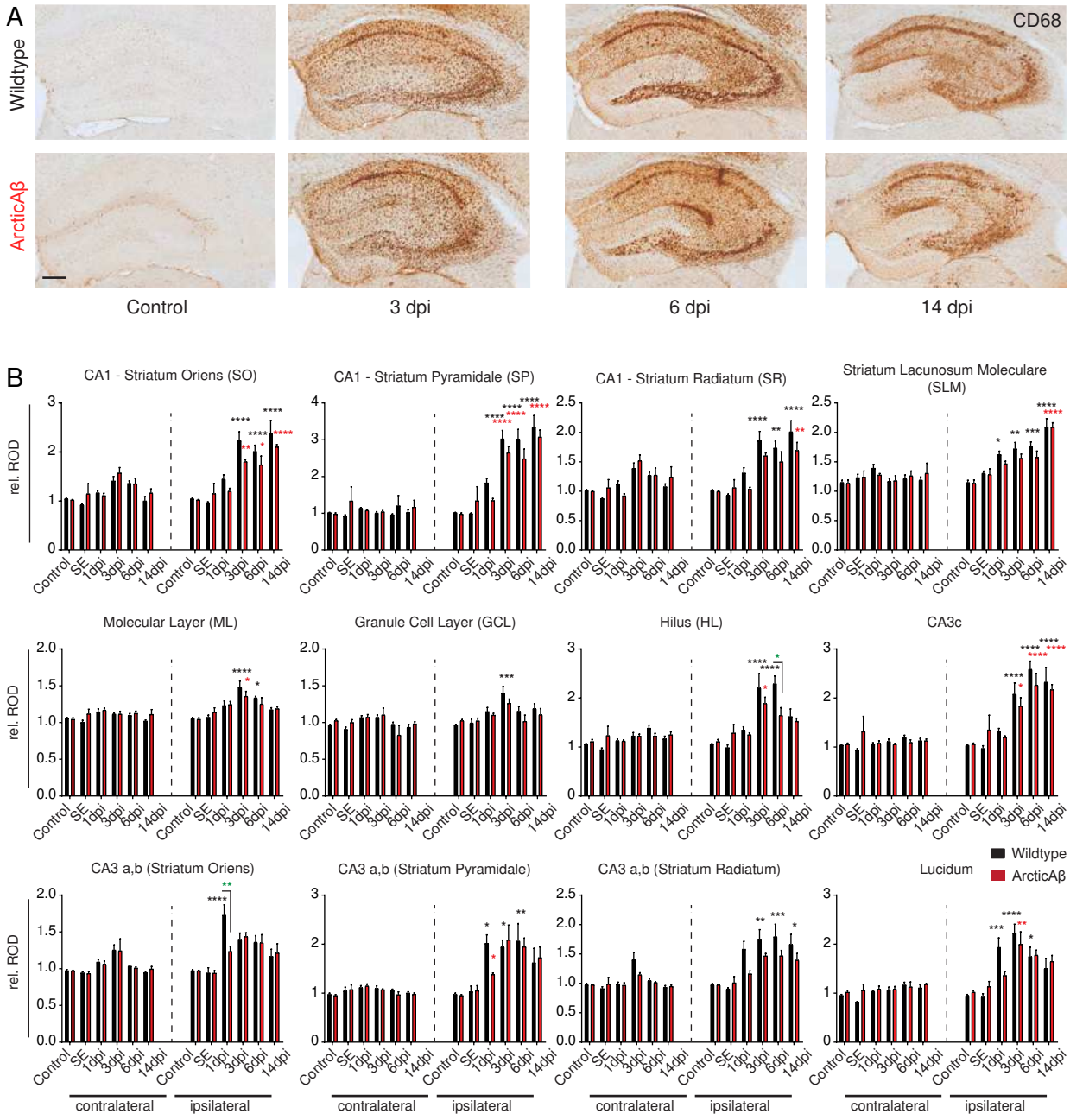
A
Wildtype
ArcticAβ
CD68
Control
3 dpi
6 dpi
14 dpi
B
CA1 - Striatum Oriens (SO)
CA1 - Striatum Pyramidale (SP)
CA1 - Striatum Radiatum (SR)
Striatum Lacunosum Moleculare (SLM)
Molecular Layer (ML)
Granule Cell Layer (GCL)
Hilus (HL)
CA3c
CA3 a,b (Striatum Oriens)
CA3 a,b (Striatum Pyramidale)
CA3 a,b (Striatum Radiatum)
Lucidum
rel. ROD
Control
SE
1dpi
3dpi
6dpi
14dpi
contralateral
ipsilateral
Wildtype
ArcticAβ

Figure 6

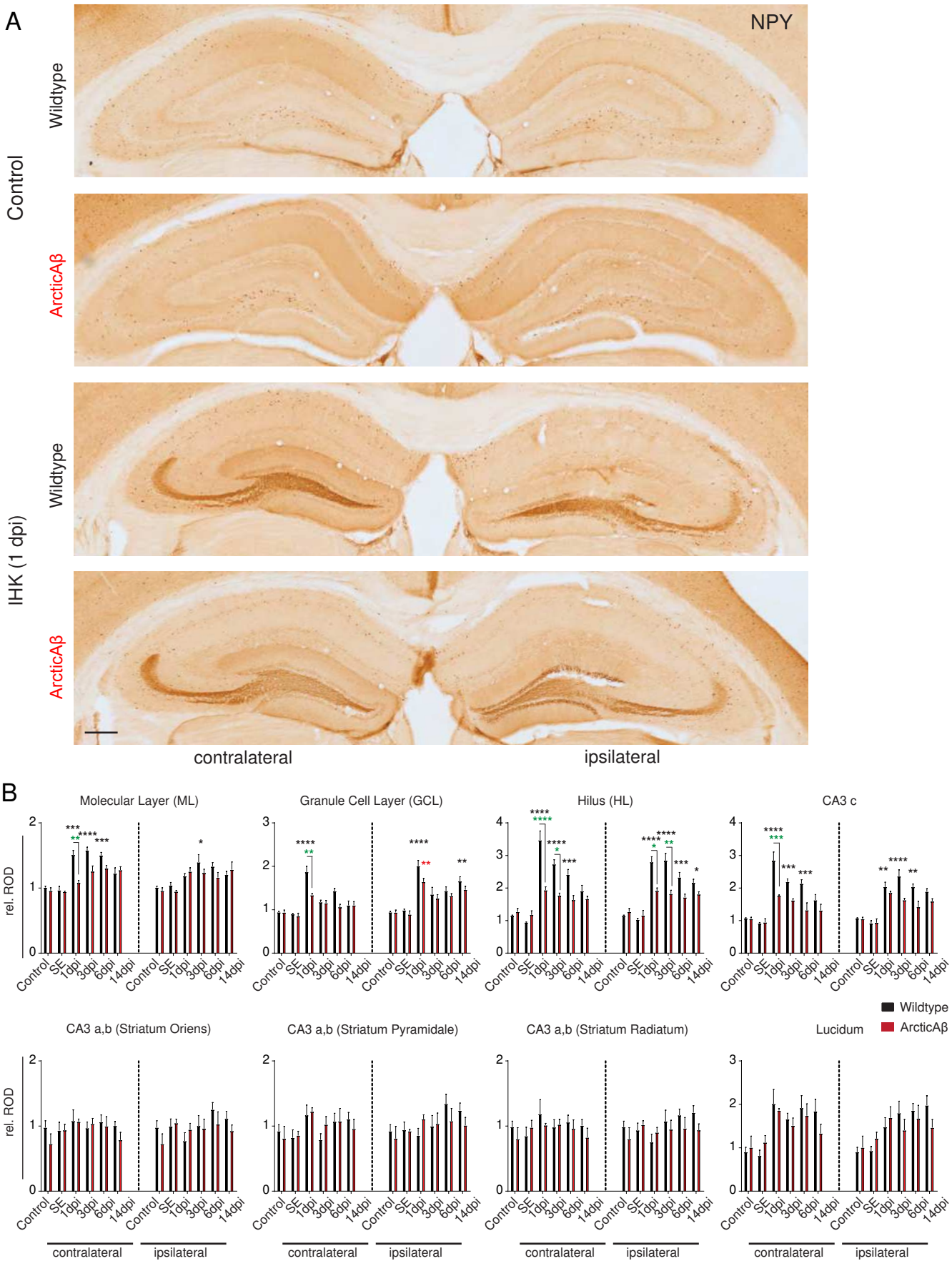
A
NPY
Control
IHK (1 dpi)
Wildtype
ArcticAβ
Wildtype
ArcticAβ
contralateral
ipsilateral
B
Molecular Layer (ML)
Granule Cell Layer (GCL)
Hilus (HL)
CA3 c
CA3 a,b (Striatum Oriens)
CA3 a,b (Striatum Pyramidale)
CA3 a,b (Striatum Radiatum)
Lucidum
rel. ROD
Control
SE
1dpi
3dpi
6dpi
14dpi
Wildtype
ArcticAβ
contralateral
ipsilateral

Figure 7

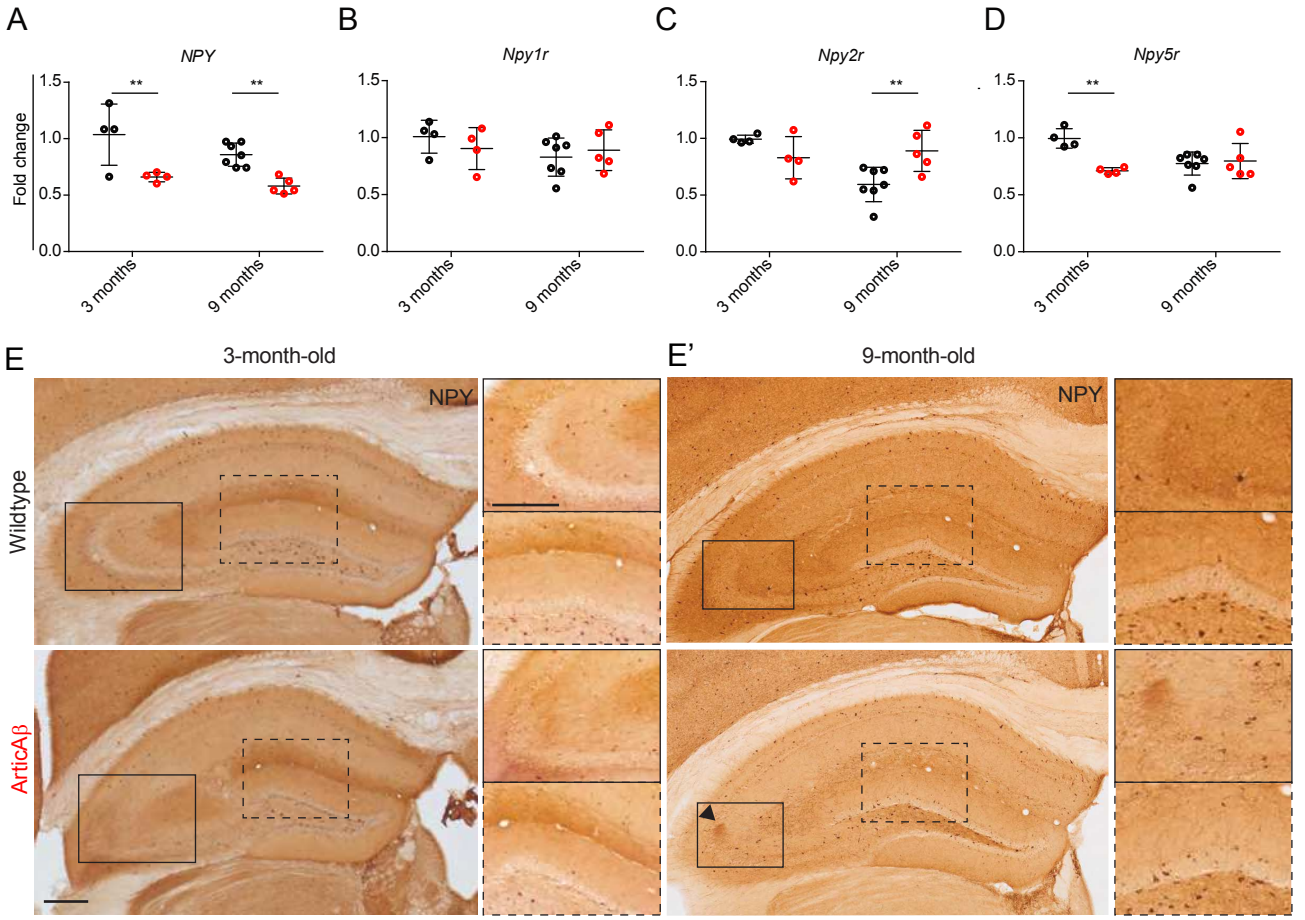
A
NPY
B
Npy1r
C
Npy2r
D
Npy5r
Fold change
1.5
1.0
0.5
0.0
**
3 months
9 months
E
3-month-old
E'
9-month-old
NPY
Wildtype
ArticAβ

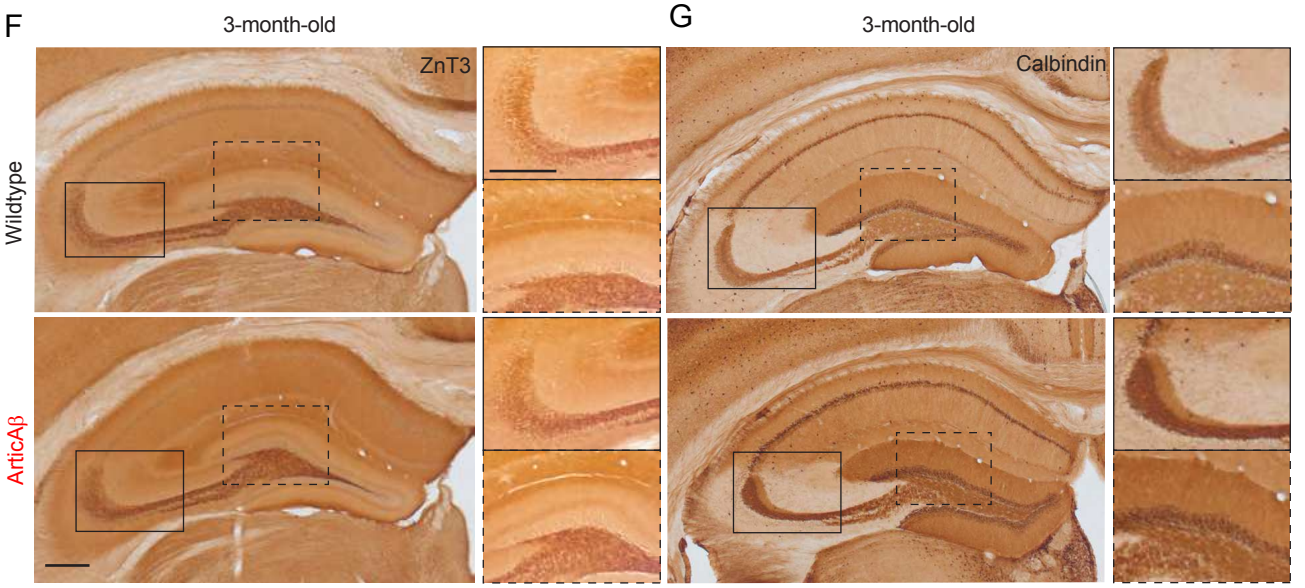
F
3-month-old
ZnT3
G
3-month-old
Calbindin
Wildtype
ArticAβ

Figure 8

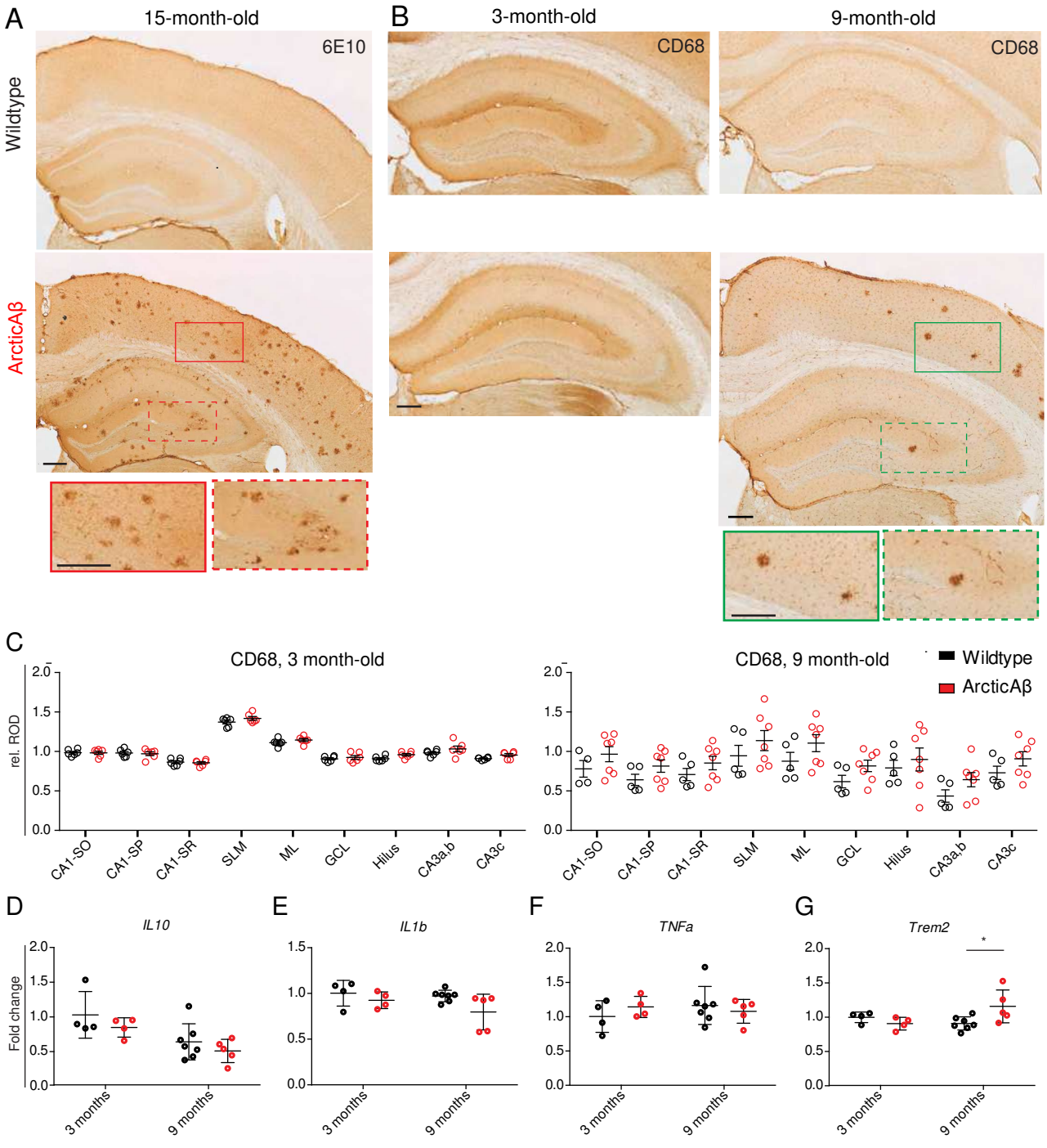
A
15-month-old
6E10
Wildtype
ArcticAβ
B
3-month-old
CD68
9-month-old
CD68
C
CD68, 3 month-old
CD68, 9 month-old
Wildtype
ArcticAβ
rel. ROD
2.0
1.5
1.0
0.5
0.0
CA1-SO
CA1-SP
CA1-SR
SLM
ML
GCL
Hilus
CA3a,b
CA3c
D
IL10
E
IL1b
F
TNFa
G
Trem2
Fold change
3 months
9 months
*

Figure 9

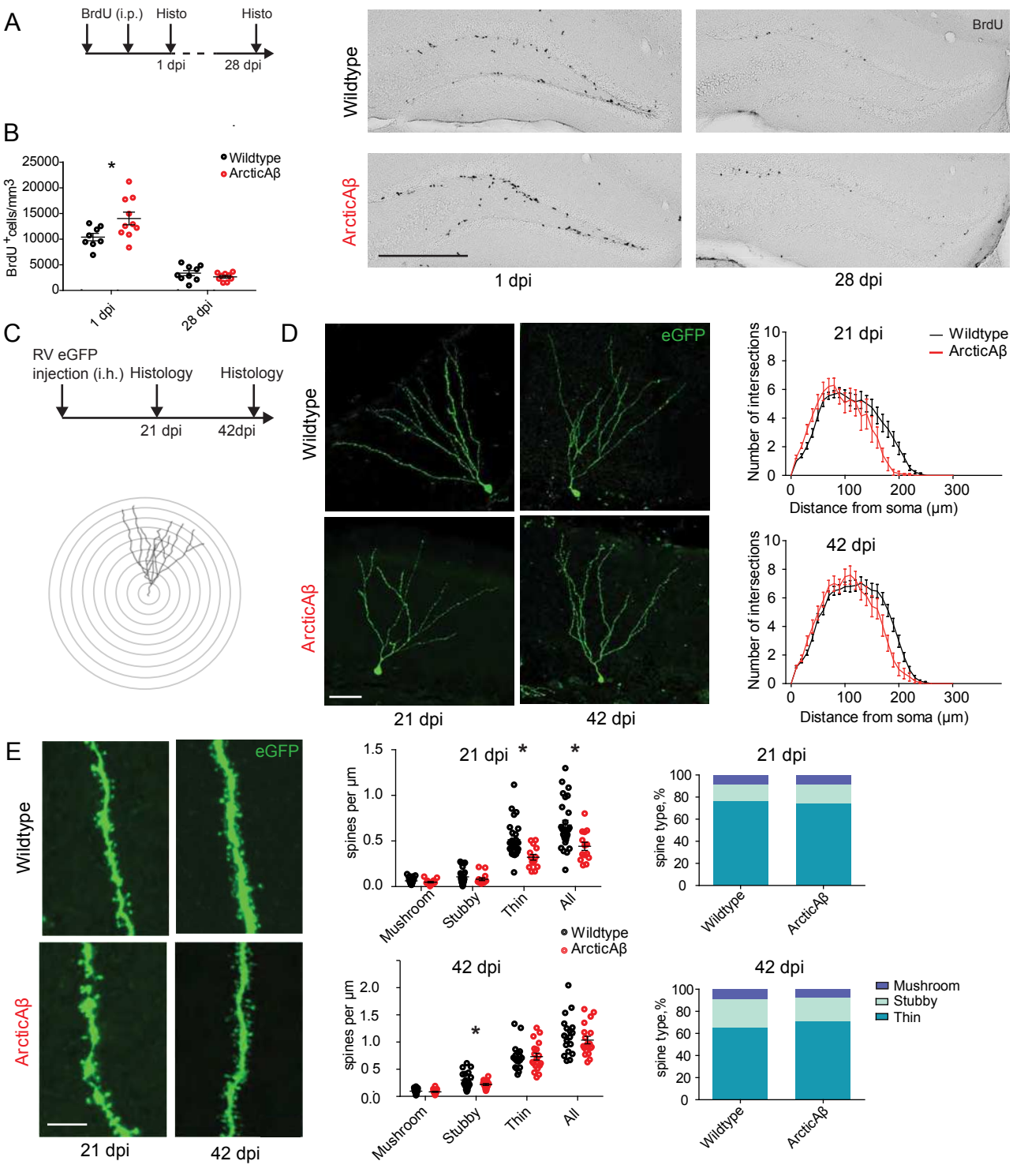
A
BrdU (i.p.)
Histo
Histo
1 dpi
28 dpi
B
Wildtype
ArcticAβ
BrdU +cells/mm3
25000
20000
15000
10000
5000
0
1 dpi
28 dpi
Wildtype
ArcticAβ
BrdU
1 dpi
28 dpi
C
RV eGFP
injection (i.h.)
Histology
Histology
21 dpi
42dpi
D
Wildtype
ArcticAβ
eGFP
21 dpi
42 dpi
21 dpi
Wildtype
ArcticAβ
Number of intersections
Distance from soma (µm)
42 dpi
Number of intersections
Distance from soma (µm)
E
Wildtype
ArcticAβ
eGFP
21 dpi
42 dpi
spines per µm
21 dpi
Mushroom
Stubby
Thin
All
Wildtype
ArcticAβ
spine type, %
21 dpi
Wildtype
ArcticAβ
42 dpi
Mushroom
Stubby
Thin
42 dpi
Wildtype
ArcticAβ

Figure 10

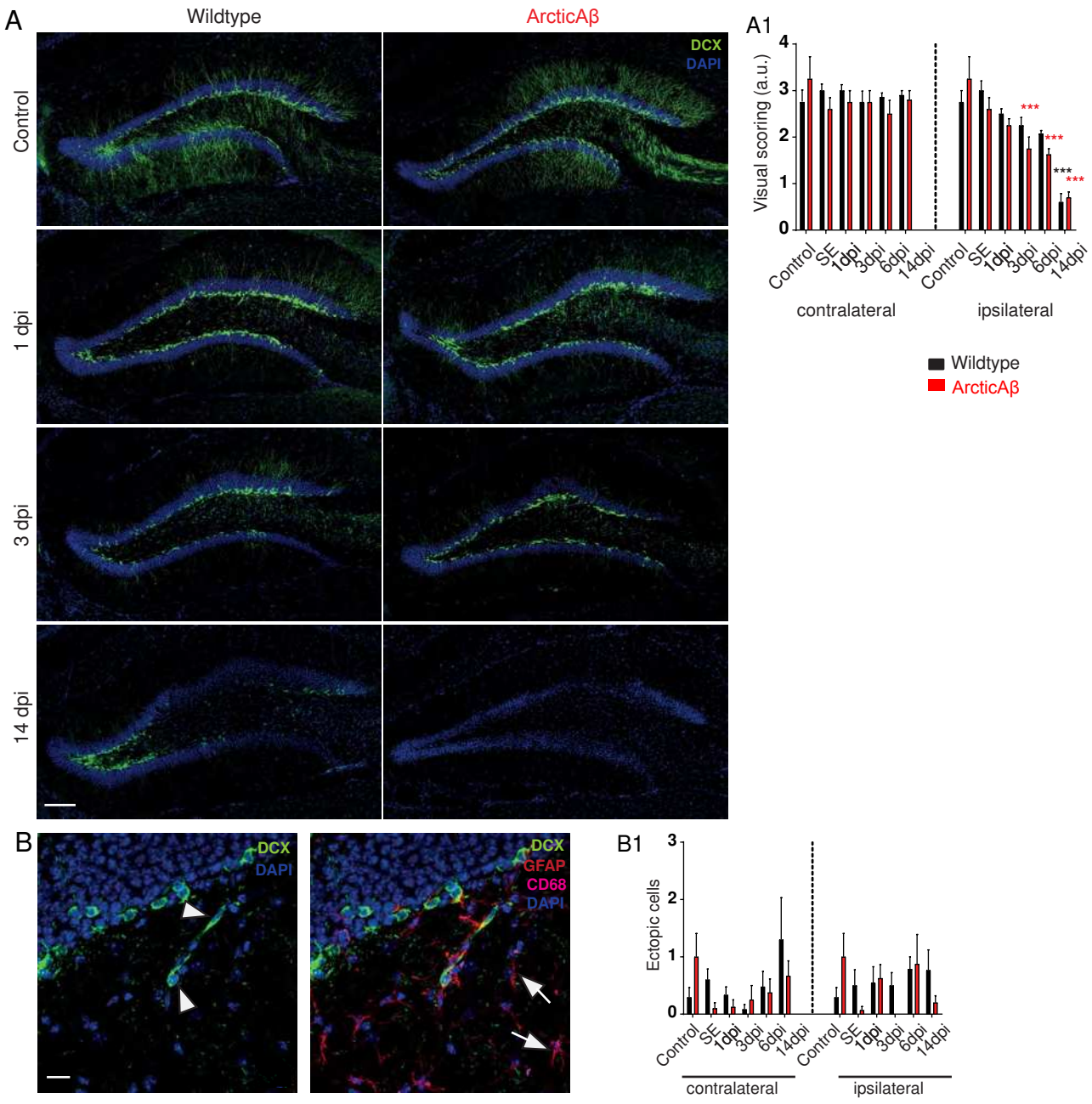
A
Wildtype
ArcticAβ
Control
1 dpi
3 dpi
14 dpi
DCX
DAPI
A1
Visual scoring (a.u.)
Control
SE
1dpi
3dpi
6dpi
14dpi
contralateral
ipsilateral
Wildtype
ArcticAβ
B
DCX
DAPI
DCX
GFAP
CD68
DAPI
B1
Ectopic cells
contralateral
ipsilateral

Figure 11

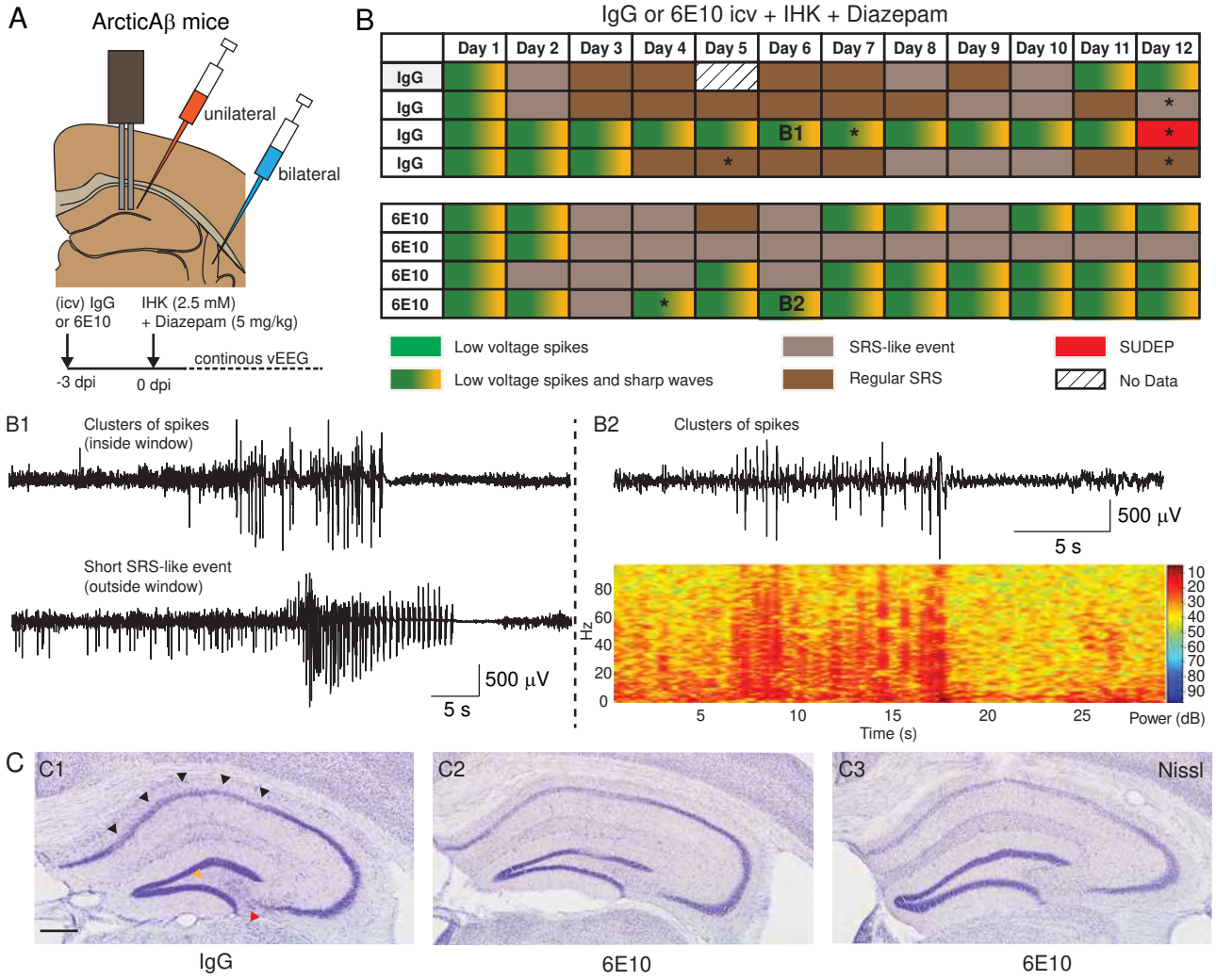
A
ArcticAβ mice
unilateral
bilateral
(icv) IgG
or 6E10
IHK (2.5 mM)
+ Diazepam (5 mg/kg)
continous vEEG
-3 dpi
0 dpi
B
IgG or 6E10 icv + IHK + Diazepam
Day 1
Day 2
Day 3
Day 4
Day 5
Day 6
Day 7
Day 8
Day 9
Day 10
Day 11
Day 12
IgG
6E10
B1
B2
Low voltage spikes
Low voltage spikes and sharp waves
SRS-like event
Regular SRS
SUDEP
No Data
B1
Clusters of spikes
(inside window)
Short SRS-like event
(outside window)
500 μV
5 s
B2
Clusters of spikes
500 μV
5 s
Hz
Time (s)
Power (dB)
C
C1
C2
C3
Nissl
IgG
6E10
6E10

Figure 12